Surface Strategies for Particulate Photocatalysts towards Artificial Photosynthesis

Shanshan Chen[1,2], Yu Qi[1], Can Li[1], Kazunari Domen[2], and Fuxiang Zhang[1,*]

[1]State Key Laboratory of Catalysis, *i*ChEM, Dalian Institute of Chemical Physics, Chinese Academy of Sciences, Dalian National Laboratory for Clean Energy, 457 Zhongshan Road, Dalian, 116023, China

[2]Department of Chemical System Engineering, School of Engineering, The University of Tokyo, 7-3-1 Hongo, Bunkyo-ku, Tokyo 113-8656, Japan

*Correspondence: fxzhang@dicp.ac.cn

Abstract: Particulate photocatalysts-based artificial photosynthesis using water as an electron donor offers a renewable and scalable way to produce solar fuels. In constructing artificial photosynthesis systems, strategies based on modifying the semiconductor surface can remarkably influence the adsorption and activation abilities of ions/molecules, the control of involved reactions, and the efficiencies of charge separation and catalytic conversion. Therefore, in this review three common ways of improving the photocatalytic performance of overall water splitting or CO_2 reduction, are summarized. Namely: (1) surface regulations by crystalline phase, crystal facet and surface defect, (2) surface functionalizations through the introduction of co-catalysts and/or a “photo-inert” metal oxide, (3) surface assembly with another semiconductor photocatalyst to form a heterostructure or an all-solid-state Z-scheme system. Challenges and future trends in the development of efficient artificial photosynthesis systems are also discussed briefly.

1. Introduction

Global fossil fuel shortages and related environmental issues have stimulated research activities towards the development of renewable and clean energy sources that do not emit carbon dioxide. Solar energy is a principle source of sustainable energy. In nature, the photosynthesis in plants transforms CO_2 and H_2O into carbohydrates and O_2 at room temperature under sunlight. Inspired by natural photosynthesis, extensive research activities have been devoted to developing artificial photosynthesis for harvesting diffuse and intermittent sunlight, and converting it to solar fuels that can be stored and transported. Overall water splitting (OWS) and CO_2 reduction with water as an electron donor are the two key processes in this field.[1,2] Both of reactions have high activation energies with an associated positive change in the Gibbs free energy.[3,4] Their similar part is the water oxidation process, while the difference is the reduction part where the proton is reduced to H_2 for OWS and CO_2 is reduced to valuable hydrocarbon chemicals for CO_2 reduction. Notably, many of the strategies adopted for OWS can be exploited for CO_2 reduction. However, photocatalytic CO_2 reduction is much more difficult to be driven than the OWS, mainly owing to the difficulty of achieving effective adsorption and activation of CO_2 molecules, and complex CO_2 reduction processes accompanying with fierce competition with the proton reduction reaction (PRR).[5,6] There are three major types of solar energy conversion systems: photovoltaic-assisted electrolysis (PV-E), photo-electrochemical (PEC) cells, and photocatalysis.[7-10] Taking water splitting for example, techno-economical analyses of the photocatalytic and PEC systems estimate that the cost of hydrogen generated by these processes would be approximately US$1.60–3.20 kg^{-1} and US$4.10–10.40 kg^{-1}, respectively.[7] Although PV-E systems can achieve the highest solar-to-hydrogen (STH) energy conversion efficiency, the price of the produced hydrogen is very expensive (about US$12.1 kg^{-1}).[9] Therefore,

particulate photocatalytic systems are the most promising way to meet the target hydrogen price of US$ 2.00–4.00 kg^{-1} set by the United States Department of Energy. However, currently, the STH efficiency achieved with this approach is the lowest among those three routes, which is below the benchmark STH value of 10%.[7] Therefore, development of highly efficient particulate water splitting photocatalysts is still the primary target in the near future.

Table 1. Potential reactions related to photocatalytic OWS and CO_2 reduction with H_2O as an electron donor.

Equation	Reaction	E^0 (V) *vs.* NHE (pH = 7)
(1)	$CO_2 + 2H^+ + 2e^- \rightarrow HCOOH$	–0.61
(2)	$CO_2 + 2H^+ + 2e^- \rightarrow CO + H_2O$	–0.53
(3)	$CO_2 + 4H^+ + 4e^- \rightarrow HCHO + H_2O$	–0.48
(4)	$2H^+ + 2e^- \rightarrow H_2$	–0.41
(5)	$CO_2 + 6H^+ + 6e^- \rightarrow CH_3OH + H_2O$	–0.38
(6)	$CO_2 + 8H^+ + 8e^- \rightarrow CH_4 + 2H_2O$	–0.24
(7)	$H_2O + 2h^+ \rightarrow 1/2O_2 + 2H^+$	0.82

For particulate photocatalytic OWS and CO_2 reduction processes, some possible reactions and the corresponding redox potentials are summarized in Table 1. It shows the target reductive product is only H_2 for OWS reaction, while there are several parallel reduction processes in CO_2 reduction reaction (CRR), and all of them compete with each other due to very similar thermodynamic requirements. To achieve those processes, there are two distinct routes, namely, one- and two-step photoexcitation routes. In one-step photo-excitation systems, the reactions of proton/CO_2 reduction and water oxidation occur on a single semiconductor photocatalyst (see Figure 1A). Generally speaking, a typical particulate photocatalytic system is composed of a light-harvesting semiconductor with particle size mainly located at the region

of 10 nm–10 μm and one or more co-catalysts with particle size of a few nanometers.[4,11,12] As a thermodynamic prerequisite, the semiconductor should have conduction band minimum (CBM) and valence band maximum (VBM) levels straddling the potentials of those redox reactions.[13-15] Chemical stability under photo-irradiation in water and sufficient carrier mobility are also necessary characteristics for these photocatalysts. However, as the bandgap of the semiconductor decreases, the driving force for the proton/CO_2 reduction reaction and/or water oxidation reaction (WOR) is reduced, making it more difficult to achieve the OWS reaction with low energy/long-wavelength visible light.[16] For a two-step photo-excitation system, it is inspired by natural photosynthesis in green plants, and is also known as the Z-scheme system. In this case, the aforementioned redox reactions are spatially separated and performed at two different functional photocatalysts (see Figure 1). It only requires the applied semiconductor photocatalyst to satisfy the band position requirement of proton/CO_2 reduction or WOR. That further means those semiconductors, which have a more negative CBM than the potential of the proton/CO_2 reduction reaction or a more positive VBM than the O_2/H_2O potential level, can be used. Thus, compared with one-step photo-excitation process, two-step system alleviates the thermodynamic requirements and expands the choice of semiconductors, making it possible to realize the water splitting/CO_2 reduction reaction with a large driving force. Here, an aqueous redox mediator or a solid-state electron mediator is necessary to complete the whole photocatalytic cycle via recombination of photo-excited electrons and holes from the water oxidation photocatalyst (WOP) and proton/CO_2 reduction photocatalyst (P/CRP), respectively. In addition, it is feasible to separate the produced reductive product and O_2 by dividing the P/CRP from the WOP.[17] Since the discovery of Honda-Fujishima effect in 1972 and the proposal of two-step photo-excitation system in 1979, considerable progress has been made in this field, especially in recent two decades.[18,19] Among the various

reported photocatalysts, some oxides, (oxy)nitrides, (oxy)sulfides and oxychlorides have been intensively investigated, accompanying with matched aqueous redox mediators or solid-state electron mediators.[20-25] Based on the valence changes of $I^{(1-/0)}$, $I^{(1-/5+)}$, $Fe^{(2+/3+)}$, $Co^{(2+/3+)}$, $V^{(4+/5+)}$, $Mn^{(2+/3+)}$ and $Mo^{(5+/6+)}$, several aqueous redox couples have been applied to two-step photo-excitation systems.[17,24,26-30] A series of electrical conductors, including Ir, Ag, Au, Rh, Ni, Pt, reduced graphene oxide (RGO) and carbon dots, have also been identified as electron mediators for solid-state two-step photo-excitation systems.[31-36] However, because of the additional elementary procedures, the number of backward electron transfer routes is increased, making this reaction scheme more complicated than the one-step photo-excitation approach.[4] Achieving effective adsorption-desorption and activation of reactants, and acceleration of the target reactions while suppressing the competing reactions, require a detailed understanding of the reaction mechanisms to enable rational design of efficient photocatalytic OWS and CO_2 reduction systems.[6,11,12]

The photocatalytic OWS and CRRs are uphill reactions when water is used as an electron donor. However, many reviews have been reported over the past decades covering the design and preparation of various heterogeneous photocatalysts for water splitting and CO_2 reduction in the presence of sacrificial reagents.[37-40] In these cases, most processes are downhill reactions associated with a negative change in the Gibbs free energy, such that photon energy is not stored. To differentiate from those reviews, this work focuses on photocatalytic OWS and CRRs with water as an electron donor, in particular those via a two-step photo-excitation route. The construction of efficient two-step photo-excited processes is challenging, involving the effective adsorption and activation of redox couples and CO_2 molecules, promotion of target reactions, inhibition of competing reactions and improvement of charge separation and catalytic conversion abilities. Note that some specific semiconductors free of co-catalyst can also act as photocatalysts, typically

composed of both a co-catalyst and a semiconductor, but the overall conversion efficiency is low due to the sluggish reaction kinetics. Co-catalyst itself can not proceed the whole photocatalytic process, due to no input of photo-generated carriers. Typically, photo-excited electrons and holes are generated in the semiconductor upon irradiation, which then transfer to the surface(s) of the semiconductor and/or co-catalyst(s) to participate in the redox reactions. Under these circumstances, the surface structure of the semiconductor plays an important role in the adsorption-desorption of reactants and products, the dispersion state of the deposited co-catalyst, and the interfacial charge transfer at the co-catalyst/semiconductor.[41-43] To address aforementioned challenges in constructing effective two-step photo-excitation processes, this review focuses on three aspects of the semiconductor surface strategies (see Figure 2). Namely: (I) surface regulation of the semiconductor (crystalline phase, crystal facet, and surface defect); (II) surface functionalizations of the semiconductor by the introduction of co-catalysts and/or a “photo-inert” metal oxide, (III) surface assembly of the semiconductor to form a heterostructure or an all-solid-state Z-scheme system. We do hope that the general methodology of surface strategies introduced in this review will give a guidance on the design and fabrication of efficient solar energy conversion systems.

2. Surface regulation of semiconductors

As shown in Figure 1, the photocatalytic Z-scheme OWS and CRRs are complicated, and involve solid, liquid, and gas phase reactants and products. Considering a typical Z-scheme OWS system with a redox couple of IO_3^-/I^- as an example, the OWS reaction is broken up into two separated parts: PRR for H_2 evolution and water oxidation for O_2 evolution (see Figure 1B). Over a H_2 evolution photocatalyst, the photo-excited electrons reduce protons to H_2 and holes oxidize I^- ions to IO_3^- ions. The IO_3^- ions are reduced back to the I^- ions

by photo-excited electrons generated over a WOP, where the holes oxidize water to O_2. Besides those targeted reactions, there also exist several competitive side reactions. IO_3^- ions reduction over a H_2 evolution photocatalyst and I^- ions oxidation over an O_2 evolution photocatalyst are backward electron transfer reactions, which need to be prohibited to ensure the H_2 and O_2 evolution reactions. In addition, competing reactions of the oxygen reduction reaction (ORR) and hydrogen oxidation reaction (HOR) also occur in the Z-scheme process.[4] Therefore, effective suppression of those side reactions is necessary to enable the Z-scheme process.[4,26] Thermodynamically, the aforementioned competing reactions are preferred over the target reactions. Kinetic control by selective adsorption/sieving of redox couple ions/molecules has been demonstrated to be an effective means of overcoming these thermodynamic constraints.[12,44] However, for the CO_2 reduction process, the adsorption and activation of CO_2 molecules are both critical steps to inhibiting competing PRR. Therefore, the construction of a semiconductor surface with the ability to adsorb and activate CO_2 molecules is desirable.[6,15] Furthermore, different surfaces exhibit distinct redox features.[45] Hence, this section will discuss the surface regulation factors of semiconductors, including the crystalline phase, crystal facet, surface defect, and their effects on the operating mechanism of Z-scheme reaction processes.

2.1. Crystalline phase

Photocatalytic conversion efficiency is highly dependent on the cumulative efficiency of the three sequential elementary steps: light absorption, charge transfer and surface reactions.[46] Semiconductors with different crystalline phases may have different electronic and band structures, which lead to differences in the efficiencies of light absorption and charge transfer. Moreover, differences in the atomic arrangements of different crystalline phases might also generate discriminative surface reactivities, which affect the selectivity of

ions/molecules adsorption and the surface catalytic reactions.[41,45] Considering TiO_2 as an example, which commonly features two crystalline phases, anatase and rutile. These two phases show completely different behaviour as WOPs in the presence of an IO_3^-/I^- couple.[26] It has been shown that the oxygen evolution reaction, which is thermodynamically less favourable than oxidation of I^- to IO_3^- (a competing reaction of the water oxidation process), proceeds preferentially over rutile TiO_2 even in the presence of I^- ions. However, such preferential water oxidation process does not take place on anatase TiO_2. The adsorption abilities of IO_3^- and I^- anions on the surfaces of anatase and rutile TiO_2 have thus been compared. Both of these anions can be adsorbed by TiO_2 particles; however, I^- ions show low adsorption to the rutile TiO_2 surface.[26] Hence, the oxidation of I^- ions is limited during the water oxidation process on the rutile TiO_2. Similar selective adsorption behaviour between IO_3^- and I^- ions is also demonstrated in the case of WO_3, although the origin of these unique adsorption characteristics has yet to be clarified. Semiconductors with different crystalline phases exhibit a diverse range of photocatalytic activities, which result from the overall behaviour in the aforementioned three elementary steps.[47] Noting that a proper surface phase junction structure formed by integrating two phases on the surface is favourable for the interfacial charge separation as well as photocatalytic performance.[48,49] Here, suppression of competing reactions (such as oxidation of I^- ions) and promotion of goal reactions (such as water oxidation) by controlling the crystalline phase of the semiconductor is one possible approach to constructing a Z-scheme system.

2.2. Crystal facet

Different crystal facets show distinct adsorption-desorption properties for ions/molecules and anisotropic surface electronic structures owing to the different atomic arrangements, even within the same semiconductor. The adsorption and activation of CO_2 and H_2O molecules on various surfaces have

been extensively studied theoretically and experimentally.[41,45] For example, using first-principles calculations He and co-workers identified that the anatase TiO_2(101) facet plays a key role in adsorbing CO_2 molecules and promoting the electron- and proton-transfer from the TiO_2 surface to CO_2 in the process of photocatalytic CO_2 reduction.[50,51] For the case of water, the key issue is whether H_2O molecules will dissociate or not, which is intrinsically determined by the coordination numbers of the surface atoms and their separation.[45] It has been theoretically and experimentally verified that the adsorption of water molecules is favourable on the anatase (101) surface with 50% Ti6c and 50% Ti5c atoms, while the dissociative adsorption of water occurs spontaneously on the anatase (001) surface with 100% Ti5c atoms.[52,53] Furthermore, semiconductors with specific exposed facets also show selective adsorption of redox couple ions. For example, rectangular shaped WO_3 particles with selectively exposed (200), (020), and (002) facets, respectively show higher and lower adsorption abilities for Fe^{3+} and Fe^{2+} ions, than commercial WO_3 samples possessing an irregular morphology.[54] These unique adsorption properties contribute to suppress the backward reaction (oxidation of Fe^{2+} ions), and enhance the photocatalytic Z-scheme OWS performance with the use of rectangular-shaped WO_3 as a WOP.

Different surface reactivities have also been demonstrated among different crystal facets.[55,56] Wang and co-workers reported that the O_2 evolution rate of $BiVO_4$ samples was enhanced as the (040)/(110) intensity ratio increased, indicating that the (040) facet plays an important role in the photocatalytic oxidation of water.[57] Theoretical calculations have suggested that the multi-atomic BiV_4 centres on the exposed (040) facet are responsible for the high O_2 evolution rate. Considering that photo-excited electrons and holes might be “attracted” to different crystal facets for the corresponding reduction and oxidation reactions, it is possible to improve the charge separation efficiency and the overall photocatalytic activity by tuning the ratio of different

facets.[55,58] Yu and co-workers prepared a series of anatase TiO_2 with different ratios of exposed {101} and {001} facets, and tested the photocatalytic CRR with H_2O vapor. Their results showed that the CH_4 evolution rate exhibited a maximum as the ratio of the exposed facets was suitably increased. Based on the density functional theory calculations, it was deduced that the photogenerated electrons and holes spontaneously migrated to {101} and {001} facets, respectively. Thus, the reduction of CO_2 to CH_4 occurred on the {101} facet, and the {001} facet provided a reaction site for water oxidation. Therefore, the redox reaction sites were spatially separated and there was a balance between these two facets owing to the charge separation and the catalytic reaction.[58] Notably, the selective accumulation of electrons or holes is not simply fixed for specific crystal facets, it also depends on the photocatalytic reduction and oxidation reactions. In addition, the spatial separation of the photogenerated electrons and holes on different facets does not occur between two arbitrary different facets. In principle, the staggered band alignments and an adequate potential difference between two facets are prerequisites for inducing charge carrier transfer. Based on this facet-induced spatially charge separation, selective deposition of reduction and oxidation co-catalysts on corresponding reduction and oxidation facets can further promote the charge separation efficiency and photocatalytic performance, as will be discussed further in section 3.[59-61]

2.3. Surface defects

Surface defects can modify the physical and chemical properties of a semiconductor surface, which are closely related to all steps in the photocatalytic process including ions/molecules adsorption-desorption and activation, intermediate products, and surface reactivity.[62] Oxygen vacancies (V_o), are common defects on the surfaces of metal oxides, which have been widely investigated for photocatalytic CO_2 reduction and OWS reactions. It has

been shown that the most stable adsorption of CO_2 molecule on rutile TiO_2(110) surface is at oxygen vacancy defect sites in a nearly linear configuration.[63] The oxygen vacancy can also help to activate and reduce CO_2 molecules. Li and co-workers reported that CO_2^- species, generated upon an electron attachment to CO_2, were spontaneously dissociated to CO even in the dark on Cu(I)/TiO_{2-x} surfaces with many V_o.[64] The formation of CO bound to Cu^+ sites was identified by *in situ* diffuse reflectance infrared Fourier transform spectroscopy. In this spontaneous dissociation process, surface V_o provide not only electronic charge for the formation of Ti^{3+} (favourable for the generation of CO_2^- species), but also sites for adsorption of oxygen atoms from CO_2.

In addition to the application of V_o to photocatalytic CO_2 reduction, these defects can also influence the photocatalytic OWS process. Takata and co-workers investigated different types of defects in $SrTiO_3$, a model OWS photocatalyst, by doping of aliovalent metal cations.[65] Note that $SrTiO_3$ is intrinsically a non-stoichiometric compound containing V_o. As indicated in equation 8, a small amount of oxygen gas forms from the dissociation of Ti-O bonds, accompanying the formation of V_o and the release of free electrons.

$$SrTiO_3 = SrTiO_{3-x} + 1/2xO_2 + 2xe^- + xV_o \quad (8)$$

$$SrTiO_3 = SrTi(IV)_{1-2x}Ti(III)_{2x}O_{3-x} + 1/2xO_2 + xV_o \quad (9)$$

$$K = [Ti^{3+}]^2[V_o]P(O_2)^{1/2} \quad (10)$$

The Ti^{4+} ions are reduced by free electrons, resulting in the creation of Ti^{3+} ions and V_o (equation 9). The density of these two defects are determined by a thermodynamic equilibrium, with the equilibrium constant K, as expressed by equation 10. As schematically illustrated in Figure 3A and B, the individual defect density of $SrTiO_3$ can be modified by aliovalent doping. The doping of a cation with a valence lower than that of the parent cation (p-doping) extrinsically introduces V_o, which inhibits the formation of Ti^{3+}. Doping of a higher valence cation (n-doping) can produce Ti^{3+}, leading to a decrease of V_o. A series of Ga- and La-doped $SrTiO_3$ have been examined, in which Ga^{3+}

occupies the Ti^{4+} site as a lower valence cation, and La^{3+} occupies the Sr^{2+} site as a higher valence cation. Notably site-selective doping was possible by the selection of suitably sized dopants according to the Goldschmidt tolerance factor, an indicator of the stability of perovskite structures.[66,67] The photocatalytic activity results showed that the doping of a lower valence cation could effectively enhance the photocatalytic activity, while doping of a higher valence cation decreased the activity (see Figure 3C). From the aforementioned analysis, it can be concluded that increase of V_o and decrease of Ti^{3+} sites improve the photocatalytic OWS activity of $SrTiO_3$.

In addition to V_o and Ti^{3+}, other defects including sulfur and nitrogen vacancies and reduced metal cations have also been reported to influence overall photocatalytic performances in some visible-light-responsive (oxy)sulfides and (oxy)nitrides.[42,68,69] Generally, several types of defects operate in a semiconductor, and clearly defining individual contributions of specific defects and their effects on the overall photocatalytic reaction process have yet to be accomplished. Appropriate surface defects can provide adsorptive sites, which benefit the activation of ions/molecules and contribute to the catalytic conversion efficiency. However, bulk defects and some other surface defects also act as charge recombination sites.[41,70] Therefore, there is generally a balance between them and an optimized condition exists when we intentionally introduce some defects to the photocatalyst. From this point of view, an in-depth understanding of the mechanism, rational creation of positive surface defects and inhibition of negative ones are highly desirable for developing efficient photocatalysts. In addition, increase of the amount of appropriate surface defects by enlarging the exposed surface area of the investigated semiconductors may be an alternative approach to further magnifying the promotion degree of the photocatalytic performance.

In this section, several approaches of crystalline phase, crystal facet and surface defect to regulate the semiconductor surface for the operation of

photocatalytic Z-scheme process are introduced, respectively. In most cases, these factors interact with each other and fine tuning of the surface structures is necessary to achieve a better photocatalytic performance.

3. Surface functionalization of semiconductors

Photocatalytic Z-scheme OWS and CRRs involve several steps including adsorption/desorption of ions/molecules, generation of photo-excited carriers, charge transfer and surface catalytic reactions. A typical photocatalyst is composed of a light harvesting semiconductor and co-catalyst(s); thus, it is difficult to achieve a highly efficient conversion process using only the aforementioned surface regulation strategies for semiconductors. The main function of the co-catalyst is to serve as a redox reaction site to catalyse the reaction by lowering the activation energy and stabilizing the photocatalyst. At the same time, the co-catalysts also trap charge carriers to promote their separation and transport.[4,11] Hence, the “reversible field”, formed by the random diffusion of photo-induced electrons and holes in particulate semiconductors, can become partially irreversible after the introduction of the co-catalyst, leading to a decreased probability of charge recombination.[12] Furthermore, competing reactions can be prohibited by finely tuning the composition and configuration of the deposited co-catalyst.[4,71] Apart from the co-catalyst, some specific “photo-inert” metal oxides can also be introduced onto semiconductor surfaces to improve the overall photocatalytic performance. This type of metal oxide does not generate photo-excited carriers upon irradiation, but instead enhances the adsorption and activation abilities of CO_2 molecules, improves the charge separation efficiency, and suppresses competing reactions.[72-74] This section focuses on these two aspects of co-catalysts and “photo-inert” metal oxides, which are deposited on the surfaces of semiconductors. We show the operating mechanisms of these two cases and their recent advances in the preparation of efficient artificial

photosynthesis systems.

3.1. Co-catalyst modification

A typical photocatalyst of co-catalyst/semiconductor is a miniaturized photo-electrochemical system, in which the co-catalyst corresponds to the counter electrode and its components typically tend to overlap with the components of the electrocatalysts.[11,75] Certain metals and metal oxide nanoparticles are frequently used as co-catalysts.[11,39,75,76] According to the redox type of the promoted reaction, the co-catalyst can be classified as a reduction or oxidation co-catalyst (see Figure 1). Generally, Pt, Rh, Ru, Ir, Au, Ag, Ni and Cu metals promote the proton/CO_2 reduction reaction, whereas oxides of Co, Fe, Mn, Ru and Ir accelerate the WOR.[13,15,37] Some specific oxides of Ni, Ir and Ru can potentially promote both the PRR and WOR, although in most cases these co-catalysts boost the PRR.[77-79] Furthermore, certain organic molecules have been shown to act as reduction and oxidation co-catalysts.[80-83] Here, the assembled molecule co-catalyst can trap the photo-excited electrons/holes from the particulate semiconductor and catalyse the corresponding reduction/oxidation reaction. Some of those systems even exhibited undiminished hydrogen evolution activity for over 300 hr.[84] Unlike the case of PRR, co-catalysts can also affect the selectivity of reductive products from the photocatalytic CRR.[85] Notably, not all co-catalysts are effective in combination with an arbitrary semiconductor in these reactions. The co-catalysts must be matched to the semiconductor in terms of their energy levels and electronic structures.[11] Hence, the co-catalyst and semiconductor should have compatible lattice and electronic structures with properly matched Fermi-levels or band levels. In this case, the interfacial charge transport process can proceed in an ideal direction between semiconductor and co-catalysts (see Figure 1), leading to efficient charge separation.

As mentioned previously, both target and competing reactions co-exist in the

photocatalytic Z-scheme OWS and CO_2 reduction systems. These two kinds of reactions competitively occur on the surfaces of the co-catalysts and semiconductors, which integrally determine the final photocatalytic performances. Therefore, it requires an effective co-catalyst should simultaneously improve target reactions and suppress competing reactions. It should be pointed out that when metallic nanoparticle is employed as a co-catalyst, a possible contribution of plasmon-induced hot electrons to the reduction of proton/CO_2 may happen. The plasmonic effect caused by the loaded metals not only affects the light absorption, but also influences the charge separation of photocatalyst. However, this kind of effect is too complicated to be well discussed during the artificial photosynthesis process, so it will not be summarized here. In this section, the main functions of co-catalyst for the improvement of desirable reactions and suppression of competing reactions will be introduced separately, although sometimes these two aspects are highly related and hard to be distinguished from each other.

3.1.1. Improvement of target reactions

As indicated above, a “matched” co-catalyst deposited on a semiconductor surface can effectively catalyse the reduction or oxidation reaction. Typically, the photogenerated electrons and holes on one photocatalyst would participate in reduction and oxidation processes, respectively. Thus, it is reasonable to deposit different functional co-catalysts to reduce the overpotentials of the corresponding redox reactions. Through this dual co-catalyst strategy, improvements of both photocatalytic activity and stability have been reported, particularly for cases of narrow bandgap (oxy)sulfides and (oxy)nitrides with weak anti-oxidation properties.[86-90] It is because the holes can be efficiently trapped by the oxidation co-catalyst that can prevent the semiconductor surface from being oxidized by holes. For example, PtO_x/WO_3 is a typical visible-light-responsive WOP with IO_3^- ions as an electron acceptor,

in which PtO_x is functioned as a reduction co-catalyst to reduce IO_3^- ions.[91] When PtO_x/WO_3 is modified with a small amount (0.001 wt %) of an oxidation co-catalyst (e.g., MnO_x, CoO_x, RuO_2 or IrO_2), the water oxidation activity is improved further. Under optimized conditions, a prepared RuO_2-PtO_x/WO_3 photocatalyst showed an apparent quantum yield (AQY) of 14.4% at 420 nm.[92] Abe and co-workers further introduced this type of photocatalyst (IrO_2-PtO_x/WO_3) to a Z-scheme OWS system, and more steady evolution of H_2 and O_2 was obtained than the case without an oxidation co-catalyst modification (PtO_x/WO_3).[93] The aforementioned dual co-catalysts were loaded by a traditional impregnation method, leading to a random distribution of deposited co-catalysts on the surface of the semiconductor. Recently, Li and co-workers showed that controlled deposition of the reduction co-catalyst on electron-accumulating sites and the oxidation co-catalyst on hole-accumulating sites can further enhance photocatalytic activity.[60] This effect can be attributed to the decreased probability of photo-excited charge carriers recombining at unmatched sites (i.e. reduction co-catalyst on hole-accumulating sites and oxidation co-catalyst on electron-accumulating sites). The selection of semiconductors with intrinsic spatial charge separation ability, such as semiconductors with anisotropic faces, is necessary for this strategy. Note that staggered band alignments and adequate potential differences between two different facets are also important for achieving spatial charge separation, as indicated in the previous section. For instance, studies of cubic $SrTiO_3$ nanocrystals with morphologies ranging from isotropic to anisotropic facets, have shown that reduction and oxidation catalytic sites can be separately distributed on anisotropic facets but are randomly distributed on isotropic facet.[61] Furthermore, controlled assembly of dual co-catalysts on the anisotropic facets of $SrTiO_3$ produced an enhanced AQY in photocatalytic OWS. This performance was approximately 6 times greater than that one of the systems based on isotropic facet. The superior performance

was attributed to the charge separation at the anisotropic facets and the spatial separation of the reduction and oxidation catalytic sites, which reduced charge recombination. In addition to semiconductors with anisotropic facets, recently a ferroelectric $PbTiO_3$ semiconductor has also been reported to possess a similar intrinsic spatial charge separation ability even without a regular morphology and facets, owing to a built-in ferroelectric field and spontaneous electric polarization in the bulk.[94] Some polar semiconductors with an internal polar electric field in the crystal structure can also be potential candidates, in which the angle between the directions of internal electric field and charge transfer is the key to determine their charge separation ability.[95]

Because co-catalysts and semiconductors have different physical and chemical properties, a new interfacial barrier is generally formed, which might influence interfacial charge transfer.[96] The interface of co-catalyst/semiconductor is the region where the photogenerated charge carriers are transferred, and is important for preventing adverse electron-hole recombination in the semiconductor. Inefficient interfacial charge transfer can limit the number of charge carriers transferred to the co-catalyst, resulting in a decreased conversion efficiency of the surface reactions. Therefore, controllable design and synthesis of the co-catalyst/semiconductor interface is desirable for efficient interfacial charge transfer, as represents an indirect approach to optimizing the co-catalyst contribution to the performance of photocatalysts.[76,97] Recently, we have demonstrated that photogenerated charge separation and water splitting performance can be greatly promoted by modifying the wettability of an interface.[42,43,98] Here, the hydrophobic surface of a Ta_3N_5 semiconductor was made hydrophilic by coating with a magnesia nanolayer (2–5 nm), leading to a great improvement of the interfacial contact between the investigated co-catalyst and the modified hydrophilic Ta_3N_5 semiconductor (see Figure 4). A series of co-catalysts including an oxidation co-catalyst of CoO_x, reduction co-catalysts of Pt and Ir were investigated in this

photocatalyst system. These results showed that the interfacial contact area between MgO/Ta_3N_5 and the co-catalyst was enlarged compared with the case of bare Ta_3N_5 without the interfacial magnesia nanolayer (see Figure 4C−F). Considering all co-catalysts were loaded by impregnation and post-annealing treatment, the improved interfacial contact can be attributed to the hydrophilic surface of the modified sample enabling uniform dispersion of the solute [such as $Co(NO_3)_2$, K_2IrCl_6, $(NH_4)_2PtCl_6$] from aqueous solution. This effect contributed to intimate interfacial contact and the deposition of co-catalysts with small particle sizes and a uniform dispersion. Furthermore, the magnesia nanolayer acted as a passivation layer to decrease surface defect sites on Ta_3N_5 and inhibit the recombination of photo-induced carriers. Time resolved infrared (TRIR) spectroscopy studies further revealed that the interfacial magnesia nanolayer could suppress the recombination of photo-induced carriers and prolong their lifetimes. Notably, when the prepared WOP of Ir-MgO/Ta_3N_5 was developed into a Z-scheme OWS system with IO_3^-/I^- as a redox couple, this sample showed a clearly decreased adsorption ability for I^- ions compared with the system without the magnesia modification. Thus, the I^- ion oxidation reaction, a competing reaction of water oxidation, was suppressed. This is one effective approach to reducing backward reactions without weakening forward reactions, as will be discussed later.

3.1.2. Suppression of competing reactions

As mentioned previously, a major obstacle to the OWS process is that the co-catalysts tend to not only promote the target reactions (PRR and WOR), but also often increase the rates of competing reactions, i.e., HOR and ORR. For the CO_2 reduction process, competing reactions of proton reduction and the re-oxidation of reductive CO_2 products also need to be prohibited. When a redox couple or solid-state electron mediator is introduced to construct a Z-scheme system, some backward electron-transfer reactions must be

avoided. As an example, for a solid-state two-step Z-scheme system, the injection of photo-excited electrons from the WOP into the solid conductor ideally completes the recombination with holes in the P/CRP. However, electrons from the P/CRP might also recombine with holes in the WOP unless a rectification function is induced.[4,96] Therefore, in most cases it appears that there is no reaction occurring or the evolved gases reflect a seriously maladjustment in the system. Thermodynamically, most competing reactions are favoured over the target reactions, making it challenging to promote the target reactions and simultaneously suppress the competing reactions. Kinetic control by selective adsorption of the redox couple ions onto the surface of semiconductors has been demonstrated to be one effective solution, as introduced in the previous section.[26,54] In this subsection, measures related to the use of co-catalysts to restrict competing reactions and their work mechanisms are introduced below.

A typical example of suppressing the competing reactions of ORR and HOR is the use of core-shell structured metal (oxide)/Cr_2O_3 reduction co-catalysts.[71,99] For example, Rh/Cr_2O_3 co-catalyst has been extensively deposited on various semiconductors for the OWS reaction. The Cr_2O_3 layer, having a thickness of several nanometres, is typically coated by a photodeposition method. In this case, the active sites of the PRR and ORR are not in the Cr_2O_3 layer but at the surface of the Rh metal. The hydrated Cr_2O_3 nanolayer enables reactants to diffuse and the formed H_2 gas to permeate to the outer surface. However, O_2 generated from water oxidation cannot permeate to the interior of the Cr_2O_3 nanolayer, which prevents O_2 from accessing the Rh-core surface, and thus limits the resulting ORR and recombination of H_2 and O_2 (see Figure 5A). The positive effect of the addition of Cr species, is not only limited to this core-shell structure, some other mixed oxides, such as $Rh_{2-y}Cr_yO_3$, also exhibit a similar behaviour.[100] It needs to be noted that the Cr component will partly loss in the long-term evaluation

process, and reloading the $Rh_{2-y}Cr_yO_3$ co-catalyst can recover the water splitting activity to a certain extent.[89] In addition to Cr-containing oxides, some similar compounds, such as Ni/NiO, Rh/La_2O_3 and Pt/MoO_3, have also been shown to be effective in restricting those competing reactions.[101-103] Recently, it has been verified that a chemisorbed molecular layer of CO on the surface of Rh co-catalyst or fluorine ions adsorbed by Pt co-catalyst can similarly function as that of Cr_2O_3 layer for OWS.[104,105] Although some extra problems are introduced, such as undesirable CO oxidation reaction, those works provide a different avenue to suppress the competing reactions. In Z-scheme systems containing aqueous redox mediators, Pt or Ru is frequently used as a reduction co-catalyst, although these noble metals are generally active for the ORR and water formation reaction. The main reason is that some of the added shuttle ions are *in situ* converted to specific species, such as the iodine layer and $[Fe(SO_4)(H_2O)_5]^+$, adsorbed on the surface of the reduction co-catalyst.[106,107] These species show similar functions to that of the Cr_2O_3 layer by restricting competing reactions. However, only some specific aqueous redox mediators have this feature and the degree of the inhibition by these *in situ* formed adsorbates is limited. It has been suggested that the use of effective Cr-containing reduction co-catalysts can further restrict competing reactions.[4,98] For example, Qi and co-workers found that the suppression of the competing reactions could be further improved by photodeposition of a thin layer of Cr_2O_3 onto the Pt surface, for the proton reduction photocatalyst (PRP) of $Pt\text{-}ZrO_2/TaON$. The obtained $Pt/Cr_2O_3\text{-}ZrO_2/TaON$ photocatalyst showed an enhanced H_2 evolution rate in the presence of the IO_3^-/I^- couple. Additionally, Abe and co-workers demonstrated that the backward electron transfer reactions could be inhibited by selective deposition of the Pt co-catalyst on interlayers of $K_4Nb_6O_{17}$.[26,93] This is a cation-exchangeable layered semiconductor, consisting of a K^+ ion interlayer and a $(Nb_6O_{17})^{4-}$ layer. Under these conditions, the oxidized species I_3^- cannot diffuse into the Pt co-catalyst

located in the interlayer spaces, owing to the electrostatic repulsion of the $(Nb_6O_{17})^{4-}$ layers. Therefore, the Pt(in)/$K_4Nb_6O_{17}$ photocatalyst can remarkably suppress the backward reaction of I_3^- reduction and acts as an effective PRP in the Z-scheme OWS system with I_3^-/I^- as a redox mediator.

In the process of CO_2 reduction with H_2O as an electron donor, the main competing reactions in OWS, such as ORR, HOR, also occur and need to be prohibited. However, its major challenges are the suppression of the PRR and the improvement of the conversion efficiency of CO_2 reduction. Generally speaking, strategies typically used for OWS can also be potentially adapted to the CO_2 reduction.[15] Wang and co-workers compared the influence of TiO_2 photocatalysts deposited with different noble metal reduction co-catalysts (e.g., Pt, Pd, Rh, Ag and Au) on photocatalytic CO_2 reduction performance. They found that the rate tendency of consumption of photogenerated electrons for the CRRs corresponded well to that for the work function of the metals. The work function reflects the electron donating or accepting ability, which increases in the order: Ag (4.26 eV) < Rh (4.98 eV) < Au (5.10 eV) < Pd (5.12 eV) < Pt (5.65 eV).[15,73,109] Among the various reductive products, the CO evolution rate was almost unchanged; however, the CH_4 evolution rate showed the highest value for the Pt/TiO_2 photocatalyst. Considering that both CO and CH_4 are formed via proton-assisted multielectron transfer reactions (equations 2 and 6), the enrichment of the electron density on Pt particles might enhance the probability of the eight-electron transfer reaction to form CH_4. However, in all these cases, the H_2 evolution rate was much higher than the evolution rate of CO or CH_4. Therefore, it is highly desirable to develop effective strategies to inhibit the PRR. For some other semiconductors, e.g., Zn-doped Ga_2O_3, $ALa_4Ti_4O_{15}$ (where A = Ca, Sr, and Ba), $La_2Ti_2O_7$, and $ZnGa_2O_4$, Ag has been shown to be an active co-catalyst for reduction of CO_2 to CO, some of which even exceeds its performance for the H_2 evolution reaction.[110-113] This is likely because Ag has a weak ability to reduce protons,

but can act as an efficient electrocatalyst for electrochemical reduction of CO_2 to form CO selectively in an aqueous $KHCO_3$ solution.[114] Besides those single metal co-catalysts, some other composites, metal-organic frameworks (MOFs), organic molecules and even bacteria have also been investigated as CO_2 reduction co-catalysts to improve conversion efficiency while suppressing competing reactions.[108,115-119] As an example, Cu is an active electrocatalyst for the reduction of CO_2 to hydrocarbons; however, its ability to extract electrons from a semiconductor is weak owing to its relatively low work function. A core-shell structured Pt/Cu_2O co-catalyst was thus designed and loaded onto the surface of the TiO_2 semiconductor.[108] Results showed that this co-catalyst could considerably promote the photocatalytic reduction of CO_2 with H_2O to CH_4 and CO, while suppressing the PRR. Detailed mechanistic investigations have revealed that the Pt core extracts photogenerated electrons from TiO_2, while the Cu_2O shell provides sites for preferential activation and conversion of CO_2 molecules, and also prevents protons from diffusing to the Pt surface to induce the PRR (see Figure 5B). In addition, the specificity for reducing CO_2 to value-added products with high selectivity enables certain organic molecules and bacteria to be used as reduction co-catalysts with a decreased rate of H_2 evolution.[115,118] However, chemically bonding such co-catalysts with particulate semiconductors to ensure efficient charge transfer at the interface, and protecting the co-catalysts from oxidization and deactivation are challenges that have yet to be addressed.[120,121]

3.2. “Photo-inert” metal oxide modification

“Photo-inert” metal oxides anchored on the surfaces of semiconductors or photocatalysts can directly affect both the semiconductor and co-catalyst, resulting in pronounced differences in the efficiencies of charge separation and catalytic conversion. Furthermore, the added modifier can make up for

deficiencies in the adsorption and activation of ions/molecules to a certain degree for the semiconductor and co-catalyst. The main functions of “photo-inert” metal oxides are outlined in this subsection.

3.2.1. Surface defect control

Nitridation treatment at high temperatures is a typical method used to prepare visible-light-responsive (oxy)nitrides, such as TaON (E_g = 2.5 eV), Ta_3N_5 (E_g = 2.1 eV).[122,123] Under this condition defects, including metal species with a low valence state and nitrogen vacancies, are unavoidably formed on the surfaces of (oxy)nitrides. These species have been reported to be detrimental to the photocatalytic performance.[42,69,124] The deposition of an appropriate metal oxide to protect the (oxy)nitride surface from being excessively reduced has been shown to be effective for controlling such surface defects. For example, monoclinic ZrO_2 has been shown to suppress the formation of surface defects during the nitridation preparation of TaON.[72,124,125] The prepared ZrO_2/TaON loaded with appropriate co-catalyst(s) showed enhanced OWS activity in one- and two-step photo-excitation processes. This improvement is mainly attributed to the introduction of ZrO_2, which causes the interfacial tantalum cations to become more cationic after the nitridation treatment, leading to a decreased defect density of reduced tantalum species. As previously indicated, MgO is an effective modifier for Ta_3N_5 to control its surface defects.[42,126] In this case, doping of Mg at Ta sites is accompanied by substitution of N^{3-} with O^{2-} owing to the charge balance. Results show that both densities of reduced tantalum species and nitrogen vacancies decrease, while the defect density of $O_N^{\bullet}$ (an oxygen atom located at a nitrogen lattice site with single positive charge) increases after the magnesia doping treatment. Theoretical calculation results have indicated that nitrogen vacancies are responsible for the localized deep states in Ta_3N_5 that likely contribute to charge recombination; however, $O_N^{\bullet}$ can induce delocalized

shallow donor states below the CBM and reduce the number of acceptor states above the VBM, which facilitates electron migration and inhibits charge recombination.[126] Similar control of the surface defects can also be realized by the formation of a solid solution.[127]

3.2.2. Adsorption and activation of ions/CO_2 molecules

We previously discussed the preferential adsorption of IO_3^- ions rather than I^- ions for WO_3 and rutile TiO_2, which makes them be effective WOPs in the Z-scheme OWS system with the IO_3^-/I^- redox couple. However, the number of photocatalysts possessing this unique ion-adsorption property is very limited, particularly for the visible-light-responsive ones. One alternative approach is direct deposition of these oxides on the surfaces of the investigated semiconductors to suppress the competing reaction of I^- oxidation. For instance, Ir/Ta_3N_5 modified with rutile TiO_2 shows decreased I^- ion-adsorption, allowing this photocatalyst to evolve O_2 in the Z-scheme OWS system.[128] In addition to WO_3 and rutile TiO_2, recently MgO has also been found to have similar ion-adsorption features, enabling Ir-MgO/Ta_3N_5 to act as an effective WOP in the presence of the IO_3^-/I^- couple.[98]

Considering that CO_2 is an acidic molecule and basic surfaces typically feature stronger interactions and higher CO_2 uptake, construction of functional basic sites on the surface of photocatalysts is thus required to adsorb and activate CO_2 molecules.[6,15] Some semiconductors with intrinsic basic sites, such as Ga_2O_3, $KTaO_3$, Mg-In layered double hydroxides, have been used for photocatalytic CO_2 reduction in H_2O.[111,129-131] However, most semiconductors do not have such basic sites, which reduce their effectiveness for photocatalytic CRR. Therefore, some basic metal (hydro)oxides, MOFs, and organic substances with nitrogen-containing basic functional groups have been deposited on the surfaces of semiconductors to act as CO_2 adsorbents and activators.[132-136] As a typical example, Pt-MgO/TiO_2 is chosen to highlight

the function of MgO in this system (see Figure 6A−C). The introduction of MgO remarkably suppresses the PRR and accelerates the reduction of CO_2 into CH_4. It has been proposed that MgO provides basic sites for preferential chemisorption of CO_2 onto the semiconductor surface and chemisorbed CO_2 molecules can be efficiently reduced by electrons trapped on the neighbouring Pt co-catalyst. Here, the interfaces between Pt, MgO and TiO_2 are the key for this promotional effect.[15,73] In addition to MgO, a series of basic metal oxides have also been investigated in the Pt/TiO_2 system to reveal a relationship between the amount of CO_2 chemisorption and the CH_4 evolution rate.[132] As shown in Figure 6D, a linear relationship was clarified, revealing that the ability to chemisorb CO_2 is important for photocatalytic CO_2 reduction to CH_4. In addition, the introduction of bases, such as hydrogen carbonate, to the aqueous reaction solution has also proved to be effective for promoting the CO_2 reduction process.[137] Notably, the formed reductive products need to be further confirmed to derive from CO_2 and H_2O, when inorganic acids or organic materials are added to the reaction systems.[134,138]

3.2.3. Prohibition of competing reactions and stabilization of the photocatalyst

Recently, it has been found that a nanolayer coating of amorphous oxyhydroxides of group IV and V transition metals (Ti, Nb and Ta) can effectively suppress the ORR and stabilize the (oxy)nitride-based photocatalysts, leading to successful OWS via one- and two-step photoexcitation systems.[74,100,139] These coating layers are photodeposited from solutions of the corresponding water-soluble metal peroxides. Upon irradiation, the O^- species can be readily reduced or oxidized to the valence state of O^{2-} or O^0, respectively, leading to the formation of a thin amorphous oxyhydroxide layer coating the entire photocatalyst surface. The formed nanolayer can act as a molecular sieve to control the surface redox chemistry, similar to effects of the aforementioned Cr_2O_3 layer. Hence, H^+ and H_2O can

diffuse into the nanolayer to participate in the PRR and WOR, and the products of H_2 and O_2 can be released to the outer phase. However, the diffusion of H_2 and O_2 in the opposite direction (into the nanolayer) is effectively prevented. Therefore, the ORR, which might occur on the surfaces of the reduction co-catalyst and semiconductor, can be prevented through this unique one-way product diffusion process. This effective suppression role can even be achieved at an enhanced operational background pressure.[140] The stability of photocatalysts based on oxynitrides is also remarkably improved after coating with an oxyhydroxide nanolayer, although the details of the related mechanism remain unclear.[100,141-144] Notably, coated photocatalysts can even split water in the presence of aqueous ethanol solution, owing to the differential permeability of H_2O and ethanol molecules (see Figure 7).[74] Thus, this approach provides an important inspiration for the design of CO_2 reduction photocatalysts with the feature of inhibiting the re-oxidation of reductive products. Here, reduction co-catalysts need to be exposed to allow free diffusion of CO_2 molecules. Furthermore, species of this coating layer can also be possibly extended to basic oxides to improve the adsorption and activation abilities of CO_2 molecules. Therefore, besides the OWS reaction, it is believed this surface coating layer strategy can also be applied to CO_2 reduction and other related solar energy conversion processes.

In this section, both modifications of co-catalyst and ""photo-inert" metal oxide were introduced from the aspects of surface defect control, adsorption and activation of reactants, improvement of target reactions and suppression of competing reactions. OWS and CRRs are very challenging reactions accompanying with several competing reactions. As a whole, how to simultaneously improve target reactions and prohibit competing reactions is still a main topic to be addressed in the future. Here, surface functionalization has been demonstrated to be one of the most effective means to achieve it.

4. Surface assemblies of semiconductors

This section concerns features of semiconductor surfaces assembled with other semiconductors for efficient photocatalytic Z-scheme OWS and CO_2 reduction processes. For the individual part of P/CRP or WOP, it is expected that enhanced charge separation efficiency can be achieved in assemblies with effective heterojunction structures. For all-solid-state systems, when two different functional photocatalysts (such as PRP and WOP) are assembled together, efficient charge recombination at the interface is desirable to enable more photogenerated charge carriers to participate in the corresponding redox reactions (see Figure 1C). The principles and advances in those two aspects are illustrated in the following subsections.

4.1. Construction of heterostructure

As for semiconductors with heterostructure, electric-field-assisted charge transport from one semiconductor to the other at the interface of them with matched band alignments is expected to be achieved. This effect can improve the charge separation and increase the lifetime of charge carriers, which is normally called as heterojunction. Based on the band structure of the two semiconductors, the heterojunction can be categorized as an isotype heterojunction (p-p or n-n) or a heterotype heterojunction (p-n). Although a p-n junction is known to be more effective for charge separation, most reports of heterostructured photocatalysts involve two n-type semiconductors, owing to the rarity of p-type semiconductors in nature. For a typical heterojunction formed by two n-type semiconductors with different band energy positions and Fermi levels, electrons flow from the semiconductor with the higher Fermi energy level (semiconductor A) to the semiconductor with the lower Fermi level (semiconductor B). This electron flow leads to the formation of an electron-depletion region in semiconductor A and an electron-accumulation region in semiconductor B. Hence, a built-in electric field forms at the interface

with a potential difference between the two sides. When the Fermi levels become equilibrated at the interfacial boundary, the electron flow stops. Accordingly, band bending occurs owing to the energy difference between the interface and the bulk in the semiconductor.[145]

Two aspects need to be carefully considered to construct an effective heterojunction, namely the band alignment and the nature of the interface. In terms of the alignment of the energy levels of the two semiconductors, a heterojunction can be classified into three different types: type I (straddling alignment), type II (staggered alignment), and type III (broken alignment) (see Figure 8).[146] For a type I heterojunction, the CB and VB levels of the larger bandgap semiconductor straddle those of the narrower bandgap semiconductor. In this case, photo-excited carriers will accumulate in the semiconductor with the narrower bandgap, leading to no improvement in charge carrier separation. In a type II junction, the CB and VB levels are staggered between the two semiconductors. In this band alignment, photogenerated electrons and holes are driven to transfer in opposite directions, enabling them to be spatially separated from each other. For type III junctions, the CB level of one semiconductor lies below the VB level of the other semiconductor. Therefore, type II heterojunctions are the most effective structure for promoting spatial charge separation and decreasing the probability of charge recombination. In addition to the band alignment, the nature of the interface is also important, because it determines the interfacial transfer of photogenerated charge carriers. A low degree of structural discontinuity and strong chemical bonds across the interface with a large contact area are highly desirable for constructing heterojunctions. Proper band alignment with a sufficient potential difference and matched interface can together drive photo-excited carriers to smoothly transfer at the junction, leading to improved charge separation efficiency.[49,147]

Note that most heterostructures used for OWS and CO_2 reduction are

constructed based on ultraviolet-light-responsive oxides, which are generally prepared by annealing treatment in air.[49,148] To improve solar energy conversion efficiency, the development of visible-light-responsive semiconductors with absorption edges at longer wavelengths is highly desirable. For this purpose, some (oxy)nitrides and (oxy)sulfides are good candidates; however, most of them are thermally unstable in air.[12,16] Recently a $MgTa_2O_{6-x}N_y$/TaON heterostructure has been prepared by a one-pot nitridation approach without annealing treatment in air.[147] These results showed that the as-fabricated $MgTa_2O_{6-x}N_y$/TaON heterostructure effectively suppressed the recombination of charge carriers and improved the H_2 evolution rate. The use of this material as a H_2-evolution photocatalyst, PtO_x/WO_3 as an O_2-evolving photocatalyst and IO_3^-/I^- as a redox mediator, a Z-scheme OWS system was thus constructed and gave an AQY of 6.8% at 420 nm (see Figure 9A). Characterization of the band structure revealed the formation of a typical type II heterojunction, with the thermodynamic potential to spatially separate photogenerated carriers (see Figure 9B). A photoreductive deposition of platinum under visible light irradiation ($\lambda \geq 420$ nm) was performed to gain insight into the direction of electron transfer. As shown in Figure 9C and D, the photoreduced Pt nanoparticles were mainly deposited on the porous surface of TaON, rather than the smooth surface of $MgTa_2O_{6-x}N_y$ (E_g: 2.18 eV), demonstrating electron transfer from $MgTa_2O_{6-x}N_y$ to TaON. Notably, the one-pot nitridation route features strong interactions at the interface, leading to the formation of an intimate interfacial contact and passivation of interfacial dangling bonds contributing to a decreased defect density. These positive factors give a remarkably enhanced carrier lifetime and improved photocatalytic performance. A similar strategy has also been demonstrated in the case of a $Ta_3N_5/BaTaO_2N$ heterostructure.[149] In addition to the two-step photoexcitation systems, heterojunction structures have also been extensively applied in one-step photo-excitation systems and PEC

systems.[150-152] To further improve the efficiencies of charge separation and catalytic conversion, it is suggested that the reduction and/or oxidation co-catalyst(s) should be deposited at locations where electrons and holes are accumulated, respectively.[60]

4.2. Construction of all-solid-state Z-scheme systems

Another surface assembly approach involves the coupling of different functional photocatalysts to construct an all-solid-state Z-scheme system for OWS or CO_2 reduction (see Figure 1C). In this system, interparticle charge transfer between the P/CRP and WOP occurs either through physical contact or through a solid electron mediator. The concept of an all-solid-state Z-scheme system was proposed and verified by Tada and co-workers in 2006.[153] Later Kudo et al. developed the first example of this typed system for OWS by combining Ru/$SrTiO_3$:Rh and $BiVO_4$ photocatalysts together.[154] In this case, the two photocatalysts were in physical contact with each another, and photo-excited electrons from the CBM of the $BiVO_4$ were injected into the dopant-derived energy levels of the $SrTiO_3$:Rh to complete the interparticle charge recombination process. The interparticle charge transfer was the key step influencing the overall charge-transfer efficiency and photocatalytic performance. Therefore, improving the interfacial contact and introducing solid electron conductors are effective strategies to enhance the probability of interparticle charge recombination.[4] Note that the contact between the reported P/CRP and WOP is mainly based on electrostatic attractive forces obtained by tuning the pH value of the reaction solution.[20] It is extremely expected that new methods need to be developed to produce a more intimate contact with a large contact area between the photocatalysts. For example, to improve the interfacial contact degree, Kudo et al. developed $BiVO_4$-$SrTiO_3$:Rh composites by preparing $BiVO_4$ in the presence of $SrTiO_3$:Rh via a liquid-solid state reaction.[155] This procedure allowed intimate contact between the two

different photocatalysts, and the composite photocatalyst showed a higher activity than a simple mixture of $BiVO_4$ and $Ru/SrTiO_3$:Rh powder under neutral pH conditions. However, the activity of this system was still limited, presumably because of chemical reactions between the two photocatalysts occurring during synthesis and the low degree of control over the interparticle contact. The introduction of solid electron conductors has also been shown to be effective for promoting the interfacial recombination of charge carriers. Several conductors, such as Ir, Ag, Au, Rh, Ni, Pt, RGO and carbon dots, have been used as solid-state electron mediators.[31-36] Some of these materials have even been used to construct the Z-scheme system for visible-light-driven CRR.[156,157] Note that the selection of P/CRP and WOP is also important for achieving an effective Z-scheme process. Kudo and co-workers demonstrated that for RGO-based solid-state Z-scheme systems, one prerequisite is the presence of an overlapped onset potential for a p-typed PRP and an n-typed WOP.[22] The deposition of an appropriate co-catalyst is an effective way to drive such kind of Z-scheme process and improve the conversion efficiency.

In addition to the powder-suspension format, the all-solid-state Z-scheme system has also been applied to the powder-fixed sheet format.[33,140] In the latter case, the interparticle contact is fixed and cannot be influenced by conditions of the reaction solution, such as stirring and the pH value. Furthermore, the photocatalysts can be easily collected and replaced when required. Both these features are advantageous for the design of practical solar water-splitting units. Recently, a unique two-step OWS system has been developed, in which a mixture of PRP and WOP particles was embedded in a continuous conductive layer with mono-particle thickness.[33,140] In this case, both the PRP and WOP particles were electrically connected by a back-contact layer, such that a sufficient contact area for efficient interparticle charge transfer was obtained. After a proper post-annealing treatment to further improve the interfacial coupling, the resulting Ru/Cr_2O_3-loaded

$SrTiO_3$:La,Rh/Au/$BiVO_4$:Mo sheet efficiently split “pure” water (pH 6.8, without any pH modification) with an AQY of 33% at 419 nm and a STH conversion efficiency of 1.1% at 331 K and 10 kPa. In this case, mediating the behaviour of the interfacial charge transfer was necessary to achieve a highly efficient process, in which band bending in the space-charge layers between the PRP/conductor/WOP interfaces needs to be carefully considered.[158] To date, various oxides, oxynitrides, oxysulfides, and conductive materials have been successfully applied to this system for OWS, and it is also expected this system can be extended to other solar energy conversion processes, including CO_2 reduction and N_2 fixation.[33,139,144,158,159]

In this section, two aspects of surface assembly of semiconductor were introduced, namely construction of heterostructure and all-solid-state Z-scheme systems. Their key point is how to effectively mediate the charge transfer at the assembled interface. Recent progresses of $MgTa_2O_{6-x}N_y$/TaON heterostructure and $SrTiO_3$:La,Rh/Au/$BiVO_4$:Mo photocatalyst sheet system well shed light on this topic.

5. Summary and outlook

OWS and CRRs, are the two most challenging artificial photosynthesis reactions involved in the conversion of solar energy to chemical energy. Each reaction shares similar features in terms of photocatalyst design, which is expected to be mutually revealing. Based on the surface of semiconductor, this review details recent advances in surface control, modification, and assembly, to achieve effective photocatalytic OWS and CRRs. In particular we highlight the similar features of these two reactions and hope to inspire more readers in these areas. To date, considerable advances have been made in both research fields through in-depth mechanism investigation and controlled construction of surfaces of semiconductors and photocatalysts. At present, there are several reported successful examples of OWS processes that show

a response to visible light up to 600 nm, a maximum STH conversion efficiency of over 1%, and a longevity of more than half year.[89,100,152,158] Comparatively, the study of photocatalytic CO_2 reduction is still in its infancy, mainly because of the challenges of adsorbing and activating CO_2 molecules for catalytic conversion, and prohibiting competing reactions.[6,15] Some effective strategies applied to OWS, such as interfacial layers, surface coating layers, heterostructures, and photocatalyst sheets, show promise for application to photocatalytic CO_2 reduction to address these challenges.[33,42,74,147] Recently other technologies have been introduced and coupled with particulate photocatalytic systems, infusing this area of solar energy research with many promising new avenues for exploration. For example, surface plasmon resonance (SPR) has recently been shown to be applicable to light-harvesting materials.[160] It has been reported that OWS can be achieved over plasmonic photocatalysts, and that the conversion efficiency of CO_2 reduction can be further improved by coupling with the SPR effect.[161-164] In addition to artificial photocatalysts, some natural photosynthetic enzymes (e.g., photosystem I, photosystem II) and bacteria have also been used in conjunction with artificial photocatalysts for OWS and CRRs.[118,165-167] These hybrid systems show potential for combining the merits of both natural and artificial photosynthetic systems. Similar hybrid photocatalytic-PEC systems have also recently been developed for two-step OWS.[168,169] Owing to the spatial separation of the PRR and WOR zones by a Nafion membrane, this configuration can partly restrict competing reactions. Most notably, it is possible to use complementary wavelengths over a wide spectral range in this tandem design.

Extensive attention has been paid to research of photocatalytic OWS and CO_2 reduction. To further boost progress in these fields, several specific suggestions listed below are highly recommended. (1) The oxygen evolution rate is necessary to provide when H_2O is used as an electron donor. The balance of photogenerated electrons and holes should be confirmed by

calculating the consumption of charge carriers from the produced solar fuels and O_2. In some cases, the evolved oxygen might be unbalanced, implying that the competing reaction of ORR may occur, which needs to be avoided in the investigated reaction systems. (2) To determine whether reductive products are derived from CO_2 and not from introduced carbon impurity intermediates, it is essential to perform isotope labelling experiments with $^{13}CO_2$ as a reactant.[138,170] In addition, blank tests and different control experiments are strongly recommended for all future studies. (3) Owing to variations in experimental illumination conditions, it is necessary to use a unified solar energy conversion efficiency measured by a series of standard procedures to enable comparison of the reaction rates of photocatalysts reported by different groups. The STH conversion efficiency is widely used in the field of OWS. For the CO_2 reduction system, owing to the various reductive products in the gas and liquid phases, it is suggested that the solar-to-chemical energy conversion efficiency should be based on the single oxidative product of O_2, associated with the selectivity of reductive products.

Although considerable progress has been made over the past decades, there is still very long way to go for having the scientific and technological abilities to make artificial photosynthesis available for practical use. The primary goals in the fields of OWS and CRRs relate to rational design and construction of highly efficient and stable photocatalytic systems based on the narrow band-gap semiconductors. In this circumstance, it becomes much more important to use the surface/interface strategies to these semiconductors, because the driving force of the reactions decreases as increasing the absorption edge. Some effective strategies used in the PEC systems are highly suggested to be “grafted” to this field. The surface of photocatalysts, acting as the sites of ions/molecules adsorption and activation, the accumulation of charge carriers, and catalytic reactions, plays key roles in the overall photocatalytic performance. The properties, including acid-base,

hydrophobicity-hydrophilicity, and internal electric fields, need to be rationally designed and controlled.[171-173] Here, the precisely controlled synthesis, theoretical simulations, and advanced *in situ* time- and space-resolved characterization techniques are highly desirable to be combined to deepen our understanding to the surface catalytic reaction process.[174-176] Although the currently obtained STH values are typically around 1% in small-scale trials, which are lower than the benchmark STH value of 10%, it is time to put more effort into applied research, such as large scalable production of promising narrow-bandgap photocatalysts consisting of inexpensive and earth-abundant elements, reactor design and manufacture, and the techno-economic analysis of the whole industrial process.[177] Artificial photosynthesis for solar fuels production has a bright future for simultaneously addressing the energy crisis and environmental challenges, so it is sincerely expected that multiple collaborations in this exciting research field will speed its industrial process.

Keywords: water splitting, CO_2 reduction, photocatalysis, surface

Abbreviations used

AQY	Apparent quantum yield
CA	Contact angle
CB	Conduction band
CBM	Conduction band minimum
CRR	CO_2 reduction reaction
E_g	Semiconductor bandgap
FESEM	Filed-emission scanning electron microscopy
HOR	Hydrogen oxidation reaction
HRTEM	High resolution transmission electron microscopy
MOFs	Metal-organic frameworks

NHE	Normal hydrogen electrode
ORR	Oxygen reduction reaction
OWS	Overall water splitting
Ox	Oxidant
P/CRP	Proton/CO_2 reduction photocatalyst
PEC	Photo-electrochemical
PRP	Proton reduction photocatalyst
PRR	Proton reduction reaction
PV-E	Photovoltaic-assisted electrolysis
Red	Reductant
RGO	Reduced graphene oxide
S_{CRR}	Selectivity of CO_2 reduction reaction
SPR	Surface plasmonic resonance
STH	Solar-to-hydrogen
TEM	Transmission electron microscopy
TRIR	Time resolved infrared
VB	Valence band
VBM	Valence band maximum
V_o	Oxygen vacancies
WOP	Water oxidation photocatalyst
WOR	Water oxidation reaction

AUTHOR CONTRIBUTIONS

S.C. and F.Z. proposed the topic of this review, and wrote the manuscript. Y.Q., C.L. and K.D. discussed and revised the manuscript.

ACKNOWLEDGEMENTS

This work was financially supported by National Natural Science Foundation of China (21633009, 21522306, 21373210), and Dalian Science Foundation for

Distinguished Young Scholars. F. Zhang thanks the priority support from the "Hundred Talents Program" of Chinese Academy of Sciences.

Declaration of Interests

The authors declare no competing interests.

REFERENCES:

1. Tachibana, Y., Vayssieres, L., and Durrant, J.R. (2012). Artificial photosynthesis for solar water-splitting. Nat. Photonics *6*, 511–518.
2. Kim, D., Sakimoto, K.K., Hong, D., and Yang, P. (2015). Artificial photosynthesis for sustainable fuel and chemical production. Angew. Chem. Int. Ed. *54*, 3259–3266.
3. Li, X., Wen, J., Low, J., Fang, Y., and Yu, J. (2014). Design and fabrication of semiconductor photocatalyst for photocatalytic reduction of CO_2 to solar fuel. Sci. China Mater. *57*, 70–100.
4. Chen, S., Takata, T., and Domen, K. (2017). Particulate photocatalysts for overall water splitting. Nat. Rev. Mater. *2*, 17050.
5. Li, K., Peng, B., and Peng, T. (2016). Recent advances in heterogeneous photocatalytic CO_2 conversion to solar fuels. ACS Catal. *6*, 7485–7527.
6. Chang, X., Wang, T., and Gong, J. (2016). CO_2 photo-reduction: insights into CO_2 activation and reaction on surfaces of photocatalysts. Energy Environ. Sci. *9*, 2177–2196.
7. Pinaud, B.A., Benck, J.D., Seitz, L.C., Forman, A.J., Chen, Z., Deutsch, T.G., James, B.D., Baum, K.N., Baum, G.N., Ardo, S., et al. (2013). Technical and economic feasibility of centralized facilities for solar hydrogen production via photocatalysis and photoelectrochemistry. Energy Environ. Sci. *6*, 1983–2002.
8. Fabian, D.M., Hu, S., Singh, N., Houle, F.A., Hisatomi, T., Domen, K., Osterloh, F.E., and Ardo, S. (2015). Particle suspension reactors and materials for solar-driven water splitting. Energy Environ. Sci. *8*, 2825−2850.
9. Shaner, M.R., Atwater, H.A., Lewis, N.S., and McFarland, E.W. (2016). A comparative technoeconomic analysis of renewable hydrogen production using solar energy. Energy Environ. Sci. *9*, 2354−2371.
10. Hisatomi, T., and Domen, K. (2017). Introductory lecture: sunlight-driven water splitting and carbon dioxide reduction by heterogeneous semiconductor systems

as key processes in artificial photosynthesis. Faraday Discuss. *198*, 11−35.

11. Yang, J., Wang, D., Han, H., and Li, C. (2013). Roles of cocatalysts in photocatalysis and photoelectrocatalysis. Acc. Chem. Res. *46*, 1900–1909.
12. Takata, T., Pan, C., and Domen, K. (2015). Recent progress in oxynitride photocatalysts for visible-light-driven water splitting. Sci. Technol. Adv. Mater. *16*, 033506.
13. Kudo, A., and Miseki, Y. (2009). Heterogeneous photocatalyst materials for water splitting. Chem. Soc. Rev. *38*, 253–278.
14. Wang, X., Maeda, K., Thomas, A., Takanabe, K., Xin, G., Carlsson, J.M., Domen, K., and Antonietti, M. (2009). A metal-free polymeric photocatalyst for hydrogen production from water under visible light. Nat. Mater. *8*, 76–80.
15. Xie, S., Zhang, Q., Liu, G., and Wang, Y. (2016). Photocatalytic and photoelectrocatalytic reduction of CO_2 using heterogeneous catalysts with controlled nanostructures. Chem. Commun. *52*, 35–59.
16. Takata, T., and Domen, K. (2017). Development of non-oxide semiconductors as light harvesting materials in photocatalytic and photoelectrochemical water splitting. Dalton Trans. *46*, 10529–10544.
17. Sasaki, Y., Kato, H., and Kudo, A. (2013). $[Co(bpy)_3]^{3+/2+}$ and $[Co(phen)_3]^{3+/2+}$ electron mediators for overall water splitting under sunlight irradiation using Z-scheme photocatalyst system. J. Am. Chem. Soc. *135*, 5441–5449.
18. Fujishima, A., and Honda, K. (1972). Electrochemical photolysis of water at a semiconductor electrode. Nature, *238*, 37–38.
19. Bard, A.J. (1979). Photoelectrochemistry and heterogeneous photo-catalysis at semiconductors. J. Photochem. *10*, 59–75.
20. Kudo, A. (2011). Z-scheme photocatalyst systems for water splitting under visible light irradiation. MRS Bull. *36*, 32–38.
21. Maeda, K. (2013). Z-scheme water splitting using two different semiconductor photocatalysts. ACS Catal. *3*, 1486–1503.
22. Iwashina, K., Iwase, A. Ng, Y.H., Amal, R., and Kudo, A. (2015). Z-schematic water splitting into H_2 and O_2 using metal sulfide as a hydrogen-evolving photocatalyst and reduced graphene oxide as a solid-state electron mediator. J. Am. Chem. Soc. *137*, 604–607.
23. Fujito, H., Kunioku, H., Kato, D., Suzuki, H., Higashi, M., Kageyama, H., and Abe, R. (2016). Layered perovskite oxychloride Bi_4NbO_8Cl: a stable visible light responsive photocatalyst for water splitting. J. Am. Chem. Soc. *138*, 2082–2085.
24. Ma, G., Chen, S., Kuang, Y., Akiyama, S., Hisatomi, T., Nakabayashi, M., Shibata,

N., Katayama, M., Minegishi, T., and Domen, K. (2016). Visible light-driven Z-scheme water splitting using oxysulfide H_2 evolution photocatalysts. J. Phys. Chem. Lett. *7*, 3892–3896.

25. Wang, Y., Suzuki, H., Xie, J., Tomita, O., Martin, D.J., Higashi, M., Kong, D., Abe, R., and Tang, J. (2018). Mimicking natural photosynthesis: solar to renewable H_2 fuel synthesis by Z-scheme water splitting systems. Chem. Rev. *118*, 5201–5241.
26. Abe, R. (2011). Development of a new system for photocatalytic water splitting into H_2 and O_2 under visible light irradiation. Bull. Chem. Soc. Jpn. *84*, 1000–1030.
27. Kato, H., Sasaki, Y., Shirakura, N., and Kudo, A. (2013). Synthesis of highly active rhodium-doped $SrTiO_3$ powders in Z-scheme systems for visible-light-driven photocatalytic overall water splitting. J. Mater. Chem. A *1*, 12327–12333.
28. Tsuji, K., Tomita, O., Higashi, M., and Abe, R. (2016). Manganese-substituted polyoxometalate as an effective shuttle redox mediator in Z-scheme water splitting under visible light. ChemSusChem *9*, 2201–2208.
29. Miseki, Y., Fujiyoshi, S., Gunji, T., and Sayama, K. (2017). Photocatalytic Z-scheme water splitting for independent H_2/O_2 production via a stepwise operation employing a vanadate redox mediator under visible light. J. Phys. Chem. C *121*, 9691–9697.
30. Iwase, Y., Tomita, O., Naito, H., Higashi, M., and Abe, R. (2018). Molybdenum-substituted polyoxometalate as stable shuttle redox mediator for visible light driven Z-scheme water splitting system. J. Photochem. Photobiol., A *356*, 347–354.
31. Iwase, A., Ng, Y.H., Ishiguro, Y., Kudo, A., and Amal, R. (2011). Reduced graphene oxide as a solid-state electron mediator in Z-scheme photocatalytic water splitting under visible light. J. Am. Chem. Soc. *133*, 11054–11057.
32. Wang, Q., Hisatomi, T., Ma, S., Li, Y., and Domen, K. (2014). Core/shell structured La- and Rh-codoped $SrTiO_3$ as a hydrogen evolution photocatalyst in Z-scheme overall water splitting under visible light irradiation. Chem. Mater. *26*, 4144–4150.
33. Wang, Q., Li, Y., Hisatomi, T., Nakabayashi, M., Shibata, N., Kubota, J., and Domen, K. (2015). Z-scheme water splitting using particulate semiconductors immobilized onto metal layers for efficient electron relay. J. Catal. *328*, 308–315.
34. Kobayashi, R., Takashima, T., Tanigawa, S., Takeuchi, S., Ohtani, B., and Irie, H. (2016). A heterojunction photocatalyst composed of zinc rhodium oxide, single

crystal-derived bismuth vanadium oxide, and silver for overall pure-water splitting under visible light up to 740 nm. Phys. Chem. Chem. Phys. *18*, 27754–27760.

35. Srinivasan, N., Sakai, E., and Miyauchi, M. (2016). Balanced excitation between two semiconductors in bulk heterojunction Z-scheme system for overall water splitting. ACS Catal. *6*, 2197–2200.
36. Wu, X., Zhao, J., Wang, L., Han, M., Zhang, M., Wang, H., Huang, H., Liu, Y., and Kang, Z. (2017). Carbon dots as solid-state electron mediator for $BiVO_4$/CDs/CdS Z-scheme photocatalyst working under visible light. Appl. Catal. *B 206*, 501–509.
37. Chen, X., Shen, S., Guo, L., and Mao, S.S. (2010). Semiconductor-based photocatalytic hydrogen generation. Chem. Rev. *110*, 6503–6570.
38. Habisreutinger, S.N., Schmidt-Mende, L. and Stolarczyk, J.K. (2013). Photocatalytic reduction of CO_2 on TiO_2 and other semiconductors. Angew. Chem. Int. Ed. *52*, 7372–7408.
39. Ma, Y., Wang, X., Jia, Y., Chen, X., Han, H., and Li, C. (2014). Titanium dioxide-based nanomaterials for photocatalytic fuel generations. Chem. Rev. *114*, 9987–10043.
40. Sun, Z., Wang, H., Wu, Z., and Wang, L. (2018). g-C_3N_4 based composite photocatalysts for photocatalytic CO_2 reduction. Catal. Today *300*, 160–172.
41. Thompson, T.L., and Yates Jr., J.T. (2006). Surface science studies of the photoactivation of TiO_2—new photochemical processes. Chem. Rev. *106*, 4428–4453.
42. Chen, S., Shen, S., Liu, G., Qi, Y., Zhang, F., and Li, C. (2015). Interface engineering of CoO_x/Ta_3N_5 photocatalyst for unprecedented water oxidation performance under visible light irradiation. Angew. Chem. Int. Ed. *54*, 3047–3051.
43. Chen, S., Qi, Y., Ding, Q., Li, Z., Cui, J., Zhang, F., and Li, C. (2016). Magnesia interface nanolayer modification of Pt/Ta_3N_5 for promoted photocatalytic hydrogen production under visible light irradiation. J. Catal. *339*, 77–83.
44. Takata, T., Pan, C., and Domen, K. (2016). Design and development of oxynitride photocatalysts for overall water splitting under visible light irradiation. ChemElectroChem *3*, 31–37.
45. Liu, G., Yang, H.G., Pan, J., Yang, Y.Q., Lu, G.Q., and Cheng, H.M. (2014). Titanium dioxide crystals with tailored facets. Chem. Rev. *114*, 9559–9612.
46. Zhang, F., and Li, C. (2016). Solar to chemical energy conversion: theory and application, M. Sugiyama, K. Fujii, and S. Nakamura, eds. (Springer

Nertherlands), pp. 299–317.

47. Li, R., Weng, Y., Zhou, X., Wang, X., Mi, Y., Chong, R., Han, H., and Li, C. (2015). Achieving overall water splitting using titanium dioxide-based photocatalysts of different phases. Energy Environ. Sci. *8*, 2377–2382.
48. Zhang, J., Xu, Q., Feng, Z., Li, M., and Li, C. (2008). Importance of the relationship between surface phases and photocatalytic activity of TiO_2. Angew. Chem. Int. Ed. *47*, 1766–1769.
49. Wang, X., Xu, Q., Li, M., Shen, S., Wang, X., Wang, Y., Feng, Z., Shi, J., Han, H., and Li, C. (2012). Photocatalytic overall water splitting promoted by an α–β phase junction on Ga_2O_3. Angew. Chem. Int. Ed. *51*, 13089–13092.
50. He, H., Zapol, P., and Curtiss, L.A. (2010). A theoretical study of CO_2 anions on anatase (101) surface. J. Phys. Chem. C *114*, 21474–21481.
51. He, H., Zapol, P., and Curtiss, L.A. (2012). Computational screening of dopants for photocatalytic two-electron reduction of CO_2 on anatase (101) surfaces. Energy Environ. Sci. *5*, 6196–6205.
52. Selloni, A., Vittadini, A., and Grätzel, M. (1998). The adsorption of small molecules on the TiO_2 anatase (101) surface by first-principles molecular dynamics. Surf. Sci. *402–404*, 219–222.
53. Vittadini, A., Selloni, A., Rotzinger, F.P., and Grätzel, M. (1998). Structure and energetics of water adsorbed at TiO_2 anatase (101) and (001) surfaces. Phys. Rev. Lett. *81*, 2954–2957.
54. Tomita, O., Nitta, S., Matsuta, Y., Hosokawa, S., Higashi, M., and Abe, R. (2017). Improved photocatalytic water oxidation with Fe^{3+}/Fe^{2+} redox on rectangular-shaped WO_3 particles with specifically exposed crystal faces via hydrothermal synthesis. Chem. Lett. *46*, 221–224.
55. Pan, J., Liu, G., Lu, G.Q., and Cheng, H.M. (2011). On the true photoreactivity order of {001}, {010}, and {101} facets of anatase TiO_2 crystals. Angew. Chem. Int. Ed. *50*, 2133–2137.
56. Ma, X., Dai, Y., Guo, M., and Huang, B. (2013). Relative photooxidation and photoreduction activities of the {100}, {101}, and {001} surfaces of anatase TiO_2. Langmuir *29*, 13647–13654.
57. Wang, D., Jiang, H., Zong, X., Xu, Q., Ma, Y., Li, G., and Li, C. (2011). Crystal facet dependence of water oxidation on $BiVO_4$ sheets under visible light irradiation. Chem. Eur. J. *17*, 1275–1282.
58. Yu, J., Low, J., Xiao, W., Zhou, P., and Jaroniec, M. (2014). Enhanced photocatalytic CO_2-reduction activity of anatase TiO_2 by coexposed {001} and

{101} facets. J. Am. Chem. Soc. *136*, 8839–8842.

59. Ohno, T., Sarukawa, K., and Matsumura, M. (2002). Crystal faces of rutile and anatase TiO_2 particles and their roles in photocatalytic reactions. New J. Chem. *26*, 1167–1170.
60. Li, R., Zhang, F., Wang, D., Yang, J., Li, M., Zhu, J., Zhou, X., Han, H., and Li, C. (2013). Spatial separation of photogenerated electrons and holes among {010} and {110} crystal facets of $BiVO_4$. Nat. Commun. *4*, 1432.
61. Mu, L., Zhao, Y., Li, A., Wang, S., Wang, Z., Yang, J., Wang, Y., Liu, T., Chen, R., Zhu, J., et al. (2016). Enhancing charge separation on high symmetry $SrTiO_3$ exposed with anisotropic facets for photocatalytic water splitting. Energy Environ. Sci. *9*, 2463–2469.
62. Campbell, C.T., and Peden, C.H.F. (2005). Oxygen vacancies and catalysis on ceria surfaces. Science, *309*, 713–714.
63. Lee, J., Sorescu, D.C., and Deng, X. (2011). Electron-induced dissociation of CO_2 on TiO_2(110). J. Am. Chem. Soc. *133*, 10066–10069.
64. Liu, L., Zhao, C., and Li, Y. (2012). Spontaneous dissociation of CO_2 to CO on defective surface of Cu(I)/TiO_{2-x} nanoparticles at room temperature. J. Phys. Chem. C *116*, 7904–7912.
65. Takata, T., and Domen, K. (2009). Defect engineering of photocatalysts by doping of aliovalent metal cations for efficient water splitting. J. Phys. Chem. C *113*, 19386–19388.
66. Hwang, H.Y., Cheong, S.W., Radaelli, P.G., Marezio, M., and Batlogg, B. (1995). Lattice effects on the magnetoresistance in doped $LaMnO_3$. Phys. Rev. Lett. *75*, 914–917.
67. Liu, X., Hong, R., and Tian, C. (2009). Tolerance factor and the stability discussion of ABO_3-type Ilmenite. J. Mater. Sci.: Mater. Electron. *20*, 323–327.
68. Fujiwara, H., Hosokawa, H., Murakoshi, K., Wada, Y., Yanagida, S., Okada, T., and Kobayashi, H. (1997). Effect of surface structures on photocatalytic CO_2 reduction using quantized CdS nanocrystallites. J. Phys. Chem. B *101*, 8270–8278.
69. Wang, J., Ma, A., Li, Z., Jiang, J., Feng, J., and Zou, Z. (2015). Unraveling the mechanism of 720 nm sub-band-gap optical absorption of a Ta_3N_5 semiconductor photocatalyst: a hybrid-DFT calculation. Phys. Chem. Chem. Phys. *17*, 8166–8171.
70. Zhang, H., Cai, J., Wang, Y., Wu, M., Meng, M., Tian, Y., Li, X., Zhang, J., Zheng, L., Jiang, Z., et al. (2018). Insights into the effects of surface/bulk defects on

photocatalytic hydrogen evolution over TiO_2 with exposed {001} facets. Appl. Catal. B *220*, 126–136.

71. Maeda, K., Teramura, K., Lu, D., Saito, N., Inoue, Y., and Domen, K. (2007). Roles of Rh/Cr_2O_3 (core/shell) nanoparticles photodeposited on visible-light-responsive $(Ga_{1-x}Zn_x)(N_{1-x}O_x)$ solid solutions in photocatalytic overall water splitting. J. Phys. Chem. C *111*, 7554–7560.
72. Maeda, K., Higashi, M., Lu, D., Abe, R., and Domen, K. (2010). Efficient nonsacrificial water splitting through two-step photoexcitation by visible light using a modified oxynitride as a hydrogen evolution photocatalyst. J. Am. Chem. Soc. *132*, 5858–5868.
73. Xie, S., Wang, Y., Zhang, Q., Deng, W., and Wang, Y. (2014). MgO- and Pt-promoted TiO_2 as an efficient photocatalyst for the preferential reduction of carbon dioxide in the presence of water. ACS Catal. *4*, 3644–3653.
74. Takata, T., Pan, C., Nakabayashi, M., Shibata, N., and Domen, K. (2015). Fabrication of a core-shell-type photocatalyst via photodeposition of group IV and V transition metal oxyhydroxides: an effective surface modification method for overall water splitting. J. Am. Chem. Soc. *137*, 9627–9634.
75. Wang, D., Li, R., Zhu, J., Shi, J., Han, J., Zong, X., and Li, C. (2012). Photocatalytic water oxidation on $BiVO_4$ with the electrocatalyst as an oxidation cocatalyst: essential relations between electrocatalyst and photocatalyst. J. Phys. Chem. C *116*, 5082–5089.
76. Bai, S., Yin, W., Wang, L., Li, Z., and Xiong, Y. (2016). Surface and interface design in cocatalysts for photocatalytic water splitting and CO_2 reduction. RSC Adv. *6*, 57446–57463.
77. Kato, H., Asakura, K., and Kudo, A., (2003). Highly efficient water splitting into H_2 and O_2 over lanthanum-doped $NaTaO_3$ photocatalysts with high crystallinity and surface nanostructure. J. Am. Chem. Soc. *125*, 3082–3089.
78. Inoue, Y. (2009). Photocatalytic water splitting by RuO_2-loaded metal oxides and nitrides with d^0- and d^{10}-related electronic configurations. Energy Environ. Sci. *2*, 364–386.
79. Asai, R., Nemoto, H., Jia, Q., Saito, K., Iwase, A., and Kudo, A. (2014). A visible light responsive rhodium and antimonycodoped $SrTiO_3$ powdered photocatalyst loaded with an IrO_2 cocatalyst for solar water splitting. Chem. Commun. *50*, 2543–2546.
80. Wen, F., and Li, C. (2013). Hybrid artificial photosynthetic systems comprising semiconductors as light harvesters and biomimetic complexes as molecular

cocatalysts. Acc. Chem. Res. *46*, 2355–2364.

81. Wang, M., Han, K., Zhang, S., and Sun, L. (2015). Integration of organometallic complexes with semiconductors and other nanomaterials for photocatalytic H_2 production. Coord. Chem. Rev. *287*, 1–14.
82. Suzuki, T.M., Iwase, A., Tanaka, H., Sato, S., Kudo, A., and Morikawa, T. (2015). Z-scheme water splitting under visible light irradiation over powdered metal-complex/semiconductor hybrid photocatalysts mediated by reduced graphene oxide. J. Mater. Chem. A *3*, 13283–13290.
83. Ye, S., Chen, R., Xu, Y., Fan, F., Du, P., Zhang, F., Zong, X., Chen, T., Qi, Y., Chen, P., et al. (2016). An artificial photosynthetic system containing an inorganic semiconductor and a molecular catalyst for photocatalytic water oxidation. J. Catal. *338*, 168–173.
84. Han, Z., Qiu, F., Eisenberg, R., Holland, P.L., and Krauss, T.D. (2012). Robust photogeneration of H_2 in water using semiconductor nanocrystals and a nickel catalyst. Science *338*, 1321–1324.
85. Ishitani, O., Inoue, C., Suzuki, Y., and Ibusuki, T. (1993). Photocatalytic reduction of carbon dioxide to methane and acetic acid by an aqueous suspension of metaldeposited TiO_2. J. Photochem. Photobiol. A *72*, 269–271.
86. Yan, H., Yang, J., Ma, G., Wu, G., Zong, X., Lei, Z., Shi, J., and Li, C. (2009). Visible-light-driven hydrogen production with extremely high quantum efficiency on Pt–PdS/CdS photocatalyst. J. Catal. *266*, 165–168.
87. Maeda, K., Xiong, A., Yoshinaga, T., Ikeda, T., Sakamoto, N., Hisatomi, T., Takashima, M., Lu, D., Kanehara, M., Setoyama, T., et al. (2010). Photocatalytic overall water splitting promoted by two different cocatalysts for hydrogen and oxygen evolution under visible light. Angew. Chem. Int. Ed. *49*, 4096–4099.
88. Liu, Q., Zhou, Y., Kou, J., Chen, X., Tian, Z., Gao, J., Yan, S., and Zou, Z. (2010). High-yield synthesis of ultralong and ultrathin Zn_2GeO_4 nanoribbons toward improved photocatalytic reduction of CO_2 into renewable hydrocarbon fuel. J. Am. Chem. Soc. *132*, 14385–14387.
89. Ohno, T., Bai, L., Hisatomi, T., Maeda, K., and Domen, K. (2012). Photocatalytic water splitting using modified GaN:ZnO solid solution under visible light: long-time operation and regeneration of activity. J. Am. Chem. Soc. *134*, 8254–8259.
90. Zhang, G., Lan, Z., and Wang, X. (2017). Surface engineering of graphitic carbon nitride polymers with cocatalysts for photocatalytic overall water splitting. Chem. Sci. *8*, 5261–5274.

91. Sayama, K., Mukasa, K., Abe, R., Abe, Y., and Arakawa, H. (2001). Stoichiometric water splitting into H_2 and O_2 using a mixture of two different photocatalysts and an IO_3^-/I^- shuttle redox mediator under visible light irradiation. Chem. Commun. 2416–2417.
92. Ma, S.S.K., Maeda, K., Abe, R., and Domen, K. (2012). Visible-light-driven nonsacrificial water oxidation over tungsten trioxide powder modified with two different cocatalysts. Energy Environ. Sci. *5*, 8390–8397.
93. Abe, R., Shinmei, K., Koumura, N., Hara, K., and Ohtani, B. (2013). Visible-light-induced water splitting based on two-step photoexcitation between dye-sensitized layered niobate and tungsten oxide photocatalysts in the presence of a triiodide/iodide shuttle redox mediator. J. Am. Chem. Soc. *135*, 16872–16884.
94. Li, R., Zhao, Y., and Li, C. (2017). Spatial distribution of active sites on a ferroelectric $PbTiO_3$ photocatalyst for photocatalytic hydrogen production. Faraday Discuss. *198*, 463–472.
95. Lou, Z., Wang, P., Huang, B., Dai, Y., Qin, X., Zhang, X., Wang, Z., and Liu, Y. (2017). Enhancing charge separation in photocatalysts with internal polar electric fields. ChemPhotoChem *1*, 136–147.
96. Zhang Z., and Yates Jr., J.T. (2012). Band bending in semiconductors: chemical and physical consequences at surfaces and interfaces. Chem. Rev. *112*, 5520–5551.
97. Guevarra, D., Shinde, A., Suram, S.K., Sharp, I.D., Toma, F.M., Haber, J.A., and Gregoire, J.M. (2016). Development of solar fuels photoanodes through combinatorial integration of Ni–La–Co–Ce oxide catalysts on $BiVO_4$. Energy Environ. Sci. *9*, 565–580.
98. Qi, Y., Chen, S., Cui, J., Wang, Z., Zhang, F., and Li, C. (2018). Inhibiting competing reactions of iodate/iodide redox mediators by surface modification of photocatalysts to enable Z-scheme overall water splitting. Appl. Catal. B *224,* 579 −585.
99. Yoshida, M., Takanabe, K., Maeda, K., Ishikawa, A., Kubota, J., Sakata, Y., Ikezawa, Y., and Domen, K. (2009). Role and function of noble-metal/Cr-layer core/shell structure cocatalysts for photocatalytic overall water splitting studied by model electrodes. J. Phys. Chem. C *113*, 10151–10157.
100. Pan, C., Takata, T., Nakabayashi, M., Matsumoto, T., Shibata, N., Ikuhara, Y., and Domen, K. (2015). A complex perovskite-type oxynitride: the first photocatalyst for water splitting operable at up to 600 nm. Angew. Chem. Int. Ed.

54, 2955–2959.

101. Domen, K., Naito, S., Soma, M., Onishi, T., and Tamaru, K. (1980). Photocatalytic decomposition of water vapour on an NO-$SrTiO_3$ Catalyst. J. Chem. Soc., Chem. Commun. 543–544.
102. Yoshida, M., Maeda, K., Lu, D., Kubota, J., and Domen, K. (2013). Lanthanoid oxide layers on rhodium-loaded $(Ga_{1-x}Zn_x)(N_{1-x}O_x)$ photocatalyst as a modifier for overall water splitting under visible-light irradiation. J. Phys. Chem. C *117*, 14000 −14006.
103. Garcia-Esparza, A.T., Shinagawa, T., Ould-Chikh, S., Qureshi, M., Peng, X., Wei, N., Anjum, D.H., Clo, A., Weng, T.C., Nordlund, D., et al. (2017). An oxygen-insensitive hydrogen evolution catalyst coated by a molybdenum-based layer for overall water splitting. Angew. Chem. Int. Ed. *56*, 5780−5784.
104. Berto, T.F., Sanwald, K.E., Byers, J.P., Browning, N.D., Gutiérrez, O.Y., and Lercher, J.A. (2016). Enabling overall water splitting on photocatalysts by CO-covered noble metal co-catalysts. J. Phys. *Chem. Lett. 7*, 4358−4362.
105. Wang, M., Li, Z., Wu, Y., Ma, J., and Lu, G. (2017). Inhibition of hydrogen and oxygen reverse recombination reaction over Pt/TiO_2 by F^- ions and its impact on the photocatalytic hydrogen formation. J. Catal. *353*, 162–170.
106. Abe, R., Sayama, K., and Arakawa, H. (2003). Significant effect of iodide addition on water splitting into H_2 and O_2 over Pt-loaded TiO_2 photocatalyst: suppression of backward reaction. Chem. Phys. Lett. *371*, 360–364.
107. Kato, H., Sasaki, Y., Iwase, A., and Kudo, A. (2007). Role of iron ion electron mediator on photocatalytic overall water splitting under visible light irradiation using Z-scheme systems. Bull. Chem. Soc. Jpn. *80*, 2457–2464.
108. Zhai, Q., Xie, S., Fan, W., Zhang, Q., Wang, Y., Deng, W., and Wang, Y. (2013). Photocatalytic conversion of carbon dioxide with water into methane: platinum and copper(I) oxide co-catalysts with a core–shell structure. Angew. Chem. Int. Ed. *52*, 5776–5779.
109. Michaelson, H.B. (1977). The work function of the elements and its periodicity. J. Appl. Phys. *48*, 4729–4733.
110. Lizuka, K., Wato, T., Miseki, Y., Saito, K., and Kudo, A. (2011). Photocatalytic reduction of carbon dioxide over Ag cocatalyst-loaded $ALa_4Ti_4O_{15}$ (A=Ca, Sr, and Ba) using water as a reducing reagent. J. Am. Chem. Soc. *133*, 20863–20868.
111. Teramura, K., Wang, Z., Hosokawa, S., Sakata, Y., and Tanaka, T. (2014). A doping technique that suppresses undesirable H_2 evolution derived from overall water splitting in the highly selective photocatalytic conversion of CO_2 in and by

water. Chem. Eur. J. *20*, 9906–9909.

112. Wang, Z., Teramura, K., Hosokawa, S., and Tanaka, T. (2015). Highly efficient photocatalytic conversion of CO_2 into solid CO using H_2O as a reductant over Ag-modified $ZnGa_2O_4$. J. Mater. Chem. A *3*, 11313–11319.
113. Wang, Z., Teramura, K., Hosokawa, S., and Tanaka, T. (2015). Photocatalytic conversion of CO_2 in water over Ag-modified $La_2Ti_2O_7$. Appl. Catal. B *163*, 241–247.
114. Hori, Y., Wakebe, H., Tsukamoto, T., and Koga, O. (1994). Electrocatalytic process of CO selectivity in electrochemical reduction of CO_2 at metal electrodes in aqueous media. Electrochim. Acta *39*, 11–12.
115. Sekizawa, K., Maeda, K., Domen, K., Koike, K., and Ishitani, O. (2013). Artificial Z-scheme constructed with a supramolecular metal complex and semiconductor for the photocatalytic reduction of CO_2. J. Am. Chem. Soc. *135*, 4596–4599.
116. Wang, S., Yao, W., Lin, J., Ding, Z., and Wang, X. (2014). Cobalt imidazolate metal–organic frameworks photosplit CO_2 under mild reaction conditions. Angew. Chem. Int. Ed. *53*, 1034–1038.
117. Neaţu, Ş., Maciá-Agulló, J.A., Concepción, P., and Garcia, H. (2014). Gold−copper nanoalloys supported on TiO_2 as photocatalysts for CO_2 reduction by water. J. Am. Chem. Soc. *136*, 15969–15976.
118. Liu, C., Gallagher, J.J., Sakimoto, K.K., Nichols, E.M., Chang, C.J., Chang, M.C.Y., and Yang, P. (2015). Nanowire−bacteria hybrids for unassisted solar carbon dioxide fixation to value-added chemicals. Nano Lett. *15*, 3634–3639.
119. Sakimoto, K.K., Wong, A.B., and Yang, P. (2016). Self-photosensitization of nonphotosynthetic bacteria for solar-to-chemical production. Science *351*, 74–77.
120. Sato, S., Arai, T., Morikawa, T., Uemura, K., Suzuki, T.M., Tanaka, H., and Kajino, T. (2011). Selective CO_2 conversion to formate conjugated with H_2O oxidation utilizing semiconductor/complex hybrid photocatalysts. J. Am. Chem. Soc. *133*, 15240–15243.
121. Lian, S., Kodaimati, M.S., Dolzhnikov, D.S., Calzada, R., and Weiss, E.A. (2017). Powering a CO_2 reduction catalyst with visible light through multiple sub-picosecond electron transfers from a quantum dot. J. Am. Chem. Soc. *139*, 8931–8938.
122. Hitoki, G., Takata, T., Kondo, J.N., Hara, M., Kobayashi, H., and Domen, K. (2002). An oxynitride, TaON, as an efficient water oxidation photocatalyst under visible light irradiation ($\lambda \leq 500$ nm). Chem. Commun. 1698–1699.
123. Hitoki, G., Ishikawa, A., Takata, T., Kondo, J.N., Hara, M., and Domen, K. (2002).

Ta_3N_5 as a novel visible light-driven photocatalyst (λ < 600 nm). Chem. Lett. 736–737.

124. Maeda, K., Terashima, H., Kase, K., Higashi, M., Tabata, M., and Domen, K. (2008). Surface modification of TaON with monoclinic ZrO_2 to produce a composite photocatalyst with enhanced hydrogen evolution activity under visible light. Bull. Chem. Soc. Jpn. *81*, 927–937.
125. Maeda, K., Lu, D., and Domen, K. (2013). Direct water splitting into hydrogen and oxygen under visible light by using modified TaON photocatalysts with d^0 electronic configuration. Chem. Eur. J. *19*, 4986–4991.
126. Xie, Y., Wang, Y., Chen, Z., and Xu, X. (2016). Role of oxygen defects on the photocatalytic properties of Mg-doped mesoporous Ta_3N_5. ChemSusChem, *9*, 1403–1412.
127. Maeda, K., Lu, D., and Domen, K. (2013). Solar-driven Z-scheme water splitting using modified $BaZrO_3$–$BaTaO_2N$ solid solutions as photocatalysts. ACS Catal. *3*, 1026–1033.
128. Tabata, M., Maeda, K., Higashi, M., Lu, D., Takata, T., Abe, R., and Domen, K. (2010). Modified Ta_3N_5 powder as a photocatalyst for O_2 evolution in a two-step water splitting system with an iodate/iodide shuttle redox mediator under visible light. Langmuir *26*, 9161–9165.
129. Teramura, K., Iguchi, S., Mizuno, Y., Shishido, T., and Tanaka, T. (2012). Photocatalytic conversion of CO_2 in water over layered double hydroxides. Angew. Chem. Int. Ed. *51*, 8008–8011.
130. Li, K., Handoko, A.D., Khraisheh, M., and Tang, J. (2014). Photocatalytic reduction of CO_2 and protons using water as an electron donor over potassium tantalate nanoflakes. Nanoscale *6*, 9767–9773.
131. Iguchi, S., Teramura, K., Hosokawa, S., and Tanaka, T. (2016). Photocatalytic conversion of CO_2 in water using fluorinated layered double hydroxides as photocatalysts. Appl. Catal. A *521*, 160–167.
132. Xie, S., Wang, Y., Zhang, Q., Fan, W., Deng, W., and Wang, Y. (2013). Photocatalytic reduction of CO_2 with H_2O: significant enhancement of the activity of Pt–TiO_2 in CH_4 formation by addition of MgO. Chem. Commun. *49*, 2451–2453.
133. Meng, X., Ouyang, S., Kako, T., Li, P., Yu, Q., Wang, T., and Ye, J. (2014). Photocatalytic CO_2 conversion over alkali modified TiO_2 without loading noble metal cocatalyst. Chem. Commun. *50*, 11517–11519.
134. Liao, Y., Cao, S.W., Yuan, Y., Gu, Q., Zhang, Z., and Xue, C. (2014). Efficient CO_2 capture and photoreduction by amine-functionalized TiO_2. Chem. Eur. J. *20*,

10220–1022.

135. Zhou, H., Li, P., Liu, J., Chen, Z., Liu, L., Dontsova, D., Yan, R., Fan, T., Zhang, D., and Ye, J. (2016). Biomimetic polymeric semiconductor based hybrid nanosystems for artificial photosynthesis towards solar fuels generation *via* CO_2 reduction. Nano Energy *25*, 128–135.

136. Lu, L., Wang, B., Wang, S., Shi, Z., Yan, S., and Zou, Z. (2017). La_2O_3-modified $LaTiO_2N$ photocatalyst with spatially separated active sites achieving enhanced CO_2 reduction. Adv. Funct. Mater. 1702447.

137. Nakanishi, H., Iizuka, K., Takayama, T., Iwase, A., and Kudo, A. (2017). Highly active $NaTaO_3$-based photocatalysts for CO_2 reduction to form CO using water as the electron donor. ChemSusChem *10*, 112–118.

138. Yui, T., Kan, A., Saitoh, C., Koike, K., Ibusuki, T., and Ishitani, O. (2011). Photochemical reduction of CO_2 using TiO_2: effects of organic adsorbates on TiO_2 and deposition of Pd onto TiO_2. ACS Appl. Mater. Interfaces *3*, 2594–2600.

139. Pan, Z., Hisatomi, T., Wang, Q., Nakabayashi, M., Shibata, N., Pan, C., Takata, T., and Domen, K. (2016). Application of $LaMg_{1/3}Ta_{2/3}O_2N$ as a hydrogen evolution photocatalyst of a photocatalyst sheet for Z-scheme water splitting. Appl. Catal. A *521*, 26–33.

140. Wang, Q., Hisatomi, T., Jia, Q., Tokudome, H., Zhong, M., Wang, C., Pan, Z., Takata, T., Nakabayashi, M., Shibata, N., et al. (2016). Scalable water splitting on particulate photocatalyst sheets with a solar-to-hydrogen energy conversion efficiency exceeding 1%. Nat. Mater. *15*, 611–615.

141. Xu, J., Pan, C., Takata, T., and Domen, K. (2015). Photocatalytic overall water splitting on the perovskite-type transition metal oxynitride $CaTaO_2N$ under visible light irradiation. Chem. Commun. *51*, 7191–7194.

142. Pan, C., Takata, T., and Domen, K. (2016). Overall water splitting on the transition-metal oxynitride photocatalyst $LaMg_{1/3}Ta_{2/3}O_2N$ over a large portion of the visible-light spectrum. Chem. Eur. J. *22*, 1854–1862.

143. Pan, C., Takata, T., Kumamoto, K., Ma, S.S.K., Ueda, K., Minegishi, T., Nakabayashi, M., Matsumoto, T., Shibata, N., Ikuhara, Y., et al (2016). Band engineering of perovskite-type transition metal oxynitrides for photocatalytic overall water splitting. J. Mater. Chem. A *4*, 4544–4552.

144. Pan, Z., Hisatomi, T., Wang, Q., Chen, S., Nakabayashi, M., Shibata, N., Pan, C., Takata, T., Katayama, M., Minegishi, T., et al. (2016). Photocatalyst sheets composed of particulate $LaMg_{1/3}Ta_{2/3}O_2N$ and Mo-doped $BiVO_4$ for Z-scheme water splitting under visible light. ACS Catal. *6*, 7188–7196.

145. Yuan, Y., Ruan, L., Barber, J., Joachim Loo, S.C., and Xue, C. (2014). Hetero-nanostructured suspended photocatalysts for solar-to-fuel conversion. Energy Environ. Sci. *7*, 3934–3951.
146. Guo, L., Wang, Y., and He, T. (2016). Photocatalytic reduction of CO_2 over heterostructure semiconductors into value-added chemicals. Chem. Rec. *16*, 1918–1933.
147. Chen, S., Qi, Y., Hisatomi, T., Ding, Q., Asai, T., Li, Z., Ma, S.S.K., Zhang, F., Domen, K., and Li, C. (2015). Efficient visible-light-driven Z-scheme overall water splitting using a $MgTa_2O_{6-x}N_y$/TaON heterostructure photocatalyst for H_2 evolution. Angew. Chem. Int. Ed. *54*, 8498–8501.
148. Xi, G., Ouyang, S., and Ye, J. (2011). General synthesis of hybrid TiO_2 mesoporous “french fries” toward improved photocatalytic conversion of CO_2 into hydrocarbon fuel: a case of TiO_2/ZnO. Chem. Eur. J. *17,* 9057–9061.
149. Qi, Y., Chen, S., Li, M., Ding, Q., Li, Z., Cui, J., Dong, B., Zhang F., and Li C. (2017). Achievement of visible-light-driven Z-scheme overall water splitting using barium-modified Ta_3N_5 as a H_2-evolving photocatalyst, Chem. Sci. *8*, 437–443.
150. Kim, E.S., Nishimura, N., Magesh, G., Kim, J.Y., Jang, J.W., Jun, H., Kubota, J., Domen, K., and Lee, J.S. (2013). Fabrication of $CaFe_2O_4$/TaON heterojunction photoanode for photoelectrochemical water oxidation. J. Am. Chem. Soc. *135*, 5375–5383.
151. Zhong, M., Ma, Y., Oleynikov, P., Domen, K., and Delaunay, J.J. (2014). A conductive ZnO–ZnGaON nanowire-array-on-a-film photoanode for stable and efficient sunlight water splitting. Energy Environ. Sci. *7*, 1693–1699.
152. Kibria, M.G., Chowdhury, F.A., Zhao, S., AlOtaibi, B., Trudeau, M.L., Guo, H., and Mi, Z. (2015). Visible light-driven efficient overall water splitting using p-type metal-nitride nanowire arrays. Nat. Commun. *6*, 6797.
153. Tada, H., Mitsui, T., Kiyonaga, T., Akita, T., and Tanaka, K. (2006). All-solid-state Z-scheme in CdS–Au–TiO_2 three-component nanojunction system. Nat. Mater. *5*, 782–786.
154. Sasaki, Y., Nemoto, H., Saito, K., and Kudo, A. (2009). Solar water splitting using powdered photocatalysts driven by Z-schematic interparticle electron transfer without an electron mediator. J. Phys. Chem. C *113*, 17536–17542.
155. Jia, Q., Iwase, A., and Kudo, A. (2014). $BiVO_4$–Ru/$SrTiO_3$:Rh composite Z-scheme photocatalyst for solar water splitting. Chem. Sci. *5*, 1513–1519.
156. He, Y., Zhang, L., Teng, B., and Fan, M. (2015). New application of Z-scheme Ag_3PO_4/g-C_3N_4 composite in converting CO_2 to fuel. Environ. Sci. Technol. *49*,

649–656.

157. Iwase, A., Yoshino, S., Takayama, T., Ng, Y.H., Amal, R., and Kudo, A. (2016). Water splitting and CO_2 reduction under visible light irradiation using Z-scheme systems consisting of metal sulfides, CoO_x-loaded $BiVO_4$, and a reduced graphene oxide electron mediator J. Am. Chem. Soc. *138*, 10260−10264.
158. Wang, Q., Hisatomi, T., Suzuki, Y., Pan, Z., Seo, J., Katayama, M., Minegishi, T., Nishiyama, H., Takata, T., Seki, K., et al. (2017). Particulate photocatalyst sheets based on carbon conductor layer for efficient Z-scheme pure-water splitting at ambient pressure. J. Am. Chem. Soc. *139*, 1675–1683.
159. Sun, S., Hisatomi, T., Wang, Q., Chen, S., Ma, G., Liu, J., Nandy, S., Minegishi, T., Katayama, M., and Domen, K. (2018). Efficient redox-mediator-free Z-scheme water splitting employing oxysulfide photocatalysts under visible light. ACS Catal. *8*, 1690–1696.
160. Wu, K., Chen, J., McBride, J.R., and Lian, T. (2015). Efficient hot-electron transfer by a plasmon-induced interfacial charge-transfer transition. Science, *349*, 632–635.
161. Zhang, Z., Wang, Z., Cao, S.W., and Xue, C. (2013). Au/Pt Nanoparticle-decorated TiO_2 nanofibers with plasmon-enhanced photocatalytic activities for solar-to-fuel conversion. J. Phys. Chem. C *117*, 25939–25947.
162. Tanaka, A., Teramura, K., Hosokawa, S., Kominami, H., and Tanaka, T. (2017). Visible light-induced water splitting in an aqueous suspension of a plasmonic Au/TiO_2 photocatalyst with metal co-catalysts. Chem. Sci. *8*, 2574–2580.
163. Wang, S., Gao, Y., Qi, Y., Li, A., Fan, F., and Li, C. (2017). Achieving overall water splitting on plasmon-based solid Z-scheme photocatalysts free of redox mediators. J. Catal. *354*, 250–257.
164. Wang, S., Gao, Y., Miao, S., Liu, T., Mu, L., Li, R., Fan, F., and Li, C. (2017). Positioning the water oxidation reaction sites in plasmonic photocatalysts. J. Am. Chem. Soc. *139*, 11771–11778.
165. Wang, W., Chen, J., Li, C., and Tian, W. (2014). Achieving solar overall water splitting with hybrid photosystems of photosystem II and artificial photocatalysts. Nat. Commun. *5*, 4647.
166. Kim, Y., Shin, D., Chang, W.J., Jang, H.L., Lee, C.W., Lee, H.E., and Nam, K.T. (2015). Hybrid Z-scheme using photosystem I and $BiVO_4$ for hydrogen production. Adv. Funct. Mater. *25*, 2369–2377.
167. Passalacqua, R., Perathoner, S., and Centi, G. (2017). Semiconductor, molecular and hybrid systems for photoelectrochemical solar fuel production. J.

Energy Chem. *26*, 219–240.

168. Wang, W., Wang, H., Zhu, Q., Qin, W., Han, G., Shen, J.R., Zong, X., and Li, C. (2016). Spatially separated photosystem II and a silicon photoelectrochemical cell for overall water splitting: a natural–artificial photosynthetic hybrid. Angew. Chem. Int. Ed. *55*, 9229–9233.
169. Li, Z., Wang, W., Ding, C., Wang, Z., Liao, S., and Li, C. (2017). Biomimetic electron transport via multiredox shuttles from photosystem II to a photoelectrochemical cell for solar water splitting. Energy Environ. Sci. *10*, 765–771.
170. Liu, C., Nangle, S.N., Colón, B.C., Silver, P.A., and Nocera, D.G. (2017). ^{13}C-Labeling the carbon-fixation pathway of a highly efficient artificial photosynthetic system. Faraday Discuss. *198*, 529–537.
171. Ma, Y., Xu, Q., Zong, X., Wang, D., Wu, G., Wang, X., and Li, C. (2012). Photocatalytic H_2 production on Pt/TiO_2–SO_4^{2-} with tuned surface-phase structures: enhancing activity and reducing CO formation. Energy Environ. Sci. *5*, 6345–6351.
172. Li, L., Salvador, P.A., and Rohrer, G.S. (2014). Photocatalysts with internal electric fields. Nanoscale, *6*, 24–42.
173. Wang, Y., Bayazit, M.K., Moniz, S.J.A., Ruan, Q.,. Lau, C.C., Martsinovich, N., and Tang, J. (2017). Linker-controlled polymeric photocatalyst for highly efficient hydrogen evolution from water. Energy Environ. Sci., *10*, 1643–1651.
174. Tang, J., Durrant, J.R., and Klug, D.R. (2008). Mechanism of photocatalytic water splitting in TiO_2. Reaction of water with photoholes, importance of charge carrier dynamics, and evidence for four-hole chemistry. J. Am. Chem. Soc. *130*, 13885–13891.
175. Zhu, J., Fan, F., Chen, R., An, H., Feng, Z., and Li, C. (2015). Direct imaging of highly anisotropic photogenerated charge separations on different facets of a single $BiVO_4$ photocatalyst. Angew. Chem. Int. Ed. *54*, 9111–9114.
176. Bai, S., Jiang, J., Zhang, Q., and Xiong, Y. (2015). Steering charge kinetics in photocatalysis: intersection of materials syntheses, characterization techniques and theoretical simulations. Chem. Soc. Rev. *44*, 2893–2939.
177. Goto, Y., Hisatomi, T., Wang, Q., Higashi, T., Ishikiriyama, K., Maeda, T., Sakata, Y., Okunaka, S., Tokudome, H., Katayama, M., et al. (2018). A particulate photocatalyst water-splitting panel for large-scale solar hydrogen generation. Joule *2*, 509–520.

Figure 1. Schematic diagrams of different systems for OWS and CRRs.

(A) One-step photoexcitation system.

(B) Two-step photoexcitation system with an aqueous redox mediator.

(C) Two-step photoexcitation system with a solid-state electron mediator.

NHE, normal hydrogen electrode; E_g, semiconductor bandgap; CB, conduction band; VB, valence band; Red, reductant; Ox, oxidant; WOP, water oxidation photocatalyst; P/CRP, proton/CO_2 reduction photocatalyst; CRRs, CO_2 reduction reactions.

Figure 2. Schematic illustration of typical strategies based on the surface of a semiconductor for two-step photo-excitation processes.

Figure 3. Schematic illustration of $SrTiO_3$ doped with (A) trivalent cation or (B) pentavalent cation and (C) their typical photocatalytic water splitting activities.

In Figure 3C, filled circles, H_2; filled squares, O_2; photocatalyst, 0.3 g; co-catalyst, Rh_2O_3 + Cr_2O_3 (0.5 + 0.5 wt % loading); reaction solution, 400 mL of distilled water; light source, high pressure Hg lamp (450 W).

Source: (A–C) Reproduced with permission from Takata et al.[65] Copyright 2009, American Chemical Society.

Figure 4. Effects of magnesia nanolayer modification on the hydrophilicity-hydrophobicity of Ta_3N_5 and the dispersion of the loaded co-catalyst.

(A) Contact angle (CA) values of MgO/Ta_3N_5 samples as a function of magnesium contents.

(B) Transmission electron microscopy (TEM) image of MgO/Ta_3N_5 sample.

(C and D) High resolution transmission electron microscopy (HRTEM) images of CoO_x/Ta_3N_5-based samples without (c) and with (d) magnesia nanolayer modification.

(E and F) Field-emission scanning electron microscopy (FESEM) images and histograms of particle-size distributions (inset) from typical samples: (e) Pt/Ta_3N_5, (f) Pt-MgO/Ta_3N_5.

In Figure 4B−F, the contents of magnesium, cobalt, and platinum were 2, 1 and 2 wt %, respectively. A.S., average size.

Source: (A–D) Reproduced with permission from Chen et al.[42] Copyright 2015, Wiley-VCH. (E and F) Reproduced with permission from Chen et al.[43] Copyright 2016, Elsevier.

Figure 5. Schematic illustration of the operating mechanisms of core-shell structured (A) metal (oxide)/Cr_2O_3 co-catalyst for PRR and (B) Pt/Cu_2O co-catalyst for CRR.

PRR, proton reduction reaction; ORR, oxygen reduction reaction; CRR, CO_2 reduction reaction.

Source: (A) Reproduced with permission from Yoshida et al.[99] Copyright 2009, American Chemical Society. (B) Reproduced with permission from Zhai et al.[108] Copyright 2013, Wiley-VCH.

Figure 6. Effect of basic metal oxides modification on the Pt/TiO_2 photocatalyst for CRR.

(A and B) Illustration of the mechanism of Pt/TiO_2-based photocatalysts without (a) and with (b) MgO modification.

(C) The effect of MgO contents on the evolution rates of reductive products.

(D) Effect of basic metal oxides on the catalytic behaviours of Pt/TiO_2 catalysts for the photocatalytic reduction of CO_2 with H_2O vapor.

CRR, CO_2 reduction reaction. S_{CRR}, selectivity of CRR.

Source: (A and B) Reproduced with permission from Xie et al.[15] Copyright 2016, The Royal Society of Chemistry. (C) Reproduced with permission from Xie et al.[73] Copyright 2014, American Chemical Society. (D) Reproduced with permission from Xie et al.[132] Copyright 2013, The Royal Society of Chemistry.

Figure 7. Effect of Ta_2O_5 coating layer on the Rh_2O_3/$SrTiO_3$:Sc photocatalyst for water splitting.

(A-i and A-ii) Time courses of photocatalytic H_2 and O_2 evolution from aqueous ethanol solution on 0.5 wt % Rh_2O_3/$SrTiO_3$:Sc-based photocatalysts without (A-i) and with (A-ii)

Ta_2O_5 coating layer. Reaction conditions: 5 wt % is used for the surface layer of Ta_2O_5, 100 mg photocatalyst, aqueous ethanol solution (10 vol %, 250 mL), 300 W xenon lamp. Filled circles, H_2; filled triangles, O_2.

(B-i and B-ii) Schematic of the reaction mechanism of 0.5 wt % Rh_2O_3/$SrTiO_3$:Sc-based photocatalysts without (B-i) and with (B-ii) Ta_2O_5 coating layer in aqueous ethanol solution.

E_g, semiconductor bandgap; CB, conduction band; VB, valence band.

Source: Reproduced with permission from Takata et al.[74] Copyright 2015, American Chemical Society.

Figure 8. Schematic energy diagrams of three different types of heterojunctions: (A) type I (straddling alignment), (B) type II (staggered alignment), (C) type III (broken alignment).

Source: (A−C) Reproduced with permission from Guo et al.[146] Copyright 2016, Wiley-VCH.

Figure 9. Characterization of $MgTa_2O_{6-x}N_y$/TaON heterostructure.

(A) Photocatalytic Z-scheme OWS activities of typical PRPs. Here, $MgTa_2O_{6-x}N_y$/TaON(mix) indicates the physical mixture of $MgTa_2O_{6-x}N_y$ and TaON, and $MgTa_2O_{6-x}N_y$/TaON denotes the one-pot prepared heterostructured sample. Reaction conditions: 75 mg PRP loaded with 0.4 wt % Pt; 150 mg 0.45 wt % PtO_x/WO_3 photocatalyst; 150 mL aqueous NaI solution (1.0 mM); Pyrex top-irradiation type; 300 W xenon lamp (λ ≥ 420 nm). PRP, proton reduction photocatalyst.

(B) The estimated relative band positions of the $MgTa_2O_{6-x}N_y$/TaON heterostructure.

(C and D) FESEM images of 0.5 wt % Pt/$MgTa_2O_{6-x}N_y$/TaON photocatalyst. Pt was deposited by photoreduction method.

Source: Reproduced with permission from Chen et al.[147] Copyright 2015, Wiley-VCH.

Figures

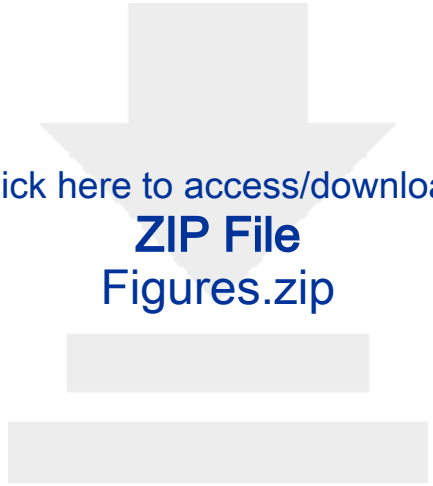

Click here to access/download

ZIP File

Figures.zip

Permissions